Chapter 4.2.2

Hydrogeologic Properties, Processes, and Alteration in the Igneous Ocean Crust

Andrew T. Fisher,[1,*] Jeffrey Alt[2] and Wolfgang Bach[3]

[1]Earth and Planetary Sciences Department, University of California, Santa Cruz, CA, USA;
[2]Department of Earth and Environmental Sciences, University of Michigan, Ann Arbor, MI, USA;
[3]Department of Geosciences, Center for Marine Environmental Sciences (MARUM), University of Bremen, Bremen, Germany
**Corresponding author: E-mail: afisher@ucsc.edu*

4.2.2.1 INTRODUCTION

4.2.2.1.1 Motivation

Fluid flow within volcanic ocean crust influences: the thermal and chemical evolution of oceanic lithosphere and seawater; subseafloor microbial ecosystems; diagenetic, seismic, and magmatic activity along plate-boundary faults; and the creation of ore deposits on and below the seafloor (e.g., Coggon, Teagle, Smith-Duque, Alt, & Cooper, 2010; Huber, Butterfield, Johnson, & Baross, 2006; Parsons & Sclater, 1977). The global hydrothermal fluid mass flux through the upper oceanic crust rivals the global riverine fluid flux to the ocean, passing the volume of the oceans through the crust every 10^5–10^6 year (e.g., Johnson & Pruis, 2003; Mottl, 2003; Wheat, McManus, Mottl, & Giambalvo, 2003). Much of this flow occurs at relatively low temperatures, far from volcanically active seafloor spreading centers where new ocean floor is created. This "ridge-flank" circulation can be influenced by off-axis volcanic or tectonic activity, and by exothermic reactions that occur within the crust during fluid transport, but most of the flow is driven by lithospheric heating from below the crust.

Fluid flow in the volcanic oceanic crust appears in several sections of the Initial Science Plan for IODP, including those focusing on solid earth cycles and alteration, ocean chemistry, and the deep biosphere. Many of the expeditions completed in the first decade of IODP operations included components of volcanic crustal hydrogeology and alteration, and several focused specifically on this topic. It is commonly assumed that time-integrated crustal hydrogeology

Developments in Marine Geology, Volume 7. http://dx.doi.org/10.1016/B978-0-444-62617-2.00018-9

is expressed in the rock record by alteration, as seen in cores and borehole measurements, and that the most recent phase(s) of water–rock interactions should be consistent with the present-day hydrogeologic state of the crust. We assess whether this assumption is valid, based on IODP results from site surveys, borehole sampling, wireline logging, monitoring and active experiments, and associated analyses of geological and biological materials. In the next section, we present a brief overview of operational and borehole measurement methods. Following sections summarize key results from selected expeditions and sites. We end with a synthesis of observational results that seeks to link hydrogeologic data to observations of crustal alteration.

4.2.2.1.2 Drilling, Coring, and Measurement Methods for the Igneous Ocean Crust

Most IODP crustal holes were drilled with a coring bit, but some were drilled without coring to improve hole stability and ease installation of casing. Some crustal holes were logged with wireline geophysical tools, to assess lithostratigraphy, hydrogeology, and rock alteration. Both core samples and geophysical logs can elucidate the physical and chemical states of the formation surrounding a borehole, which results from primary crustal construction overlain by tectonic, magmatic, and alteration (especially, hydrothermal) processes that occur as the lithosphere ages.

The most common logging tools deployed in the ocean crust include caliper (hole diameter), bulk density, porosity, resistivity, seismic velocity, and borehole temperature (we use generic logging tool descriptions throughout this chapter, rather than specific tool names and acronyms). Some basement holes have also been logged with tools that create higher-resolution images of the borehole wall using resistivity and sonic data. In general, wireline geophysical logs are the most accurate, and tools are least likely to get stuck, in holes that are "to gauge" (having a relatively uniform diameter that is slightly larger than the drill bit diameter). Good hole conditions also can contribute to higher core recovery; however, many zones in the crust, inferred to be of greatest hydrogeologic interest, are also where rocks are fractured, porous, and weak, resulting in poor core recovery and poor logging tool response.

Hydrogeologic tests of individual crustal holes drilled during IODP have been conducted using a drillstring packer system (e.g., Becker, 1986; Becker & Davis, 2004; Becker & Fisher, 2000). The IODP packer system is incorporated into the bottom-hole assembly of a drillstring. An inflateable packer element is used to hydraulically isolate part of a borehole so that pressure and fluid flow conditions can be perturbed and the formation response can be monitored. The IODP packer has been inflated in casing to test the entire open-hole interval below, and in open hole where the hole diameter is small enough and the formation is sufficiently massive to hold the inflated element and form a seal against the borehole wall. Interpretation of single-hole packer tests is based on fitting pressure-time observations

to an equation of the form: $\Delta P = f(Q,t,T)$, where Q is fluid pumping rate, t is time, and T is formation transmissivity (dimensions of L^2/T). Transmissivity is the product of aquifer thickness and hydraulic conductivity, K, within a horizontal, tabular aquifer, where the latter is related to permeability, k, as $k = K\mu/\varrho g$, μ being dynamic viscosity and ϱg being a unit weight of fluid.

Temperature logs in cased, crustal boreholes have quantified downflow and upflow conditions, and researchers have used these observations and estimated or measured differential pressures to infer near-borehole hydrogeologic properties (e.g., Becker & Davis, 2003; Becker, Langseth, Von Herzen, & Anderson, 1983; Fisher, Becker, & Davis, 1997; Winslow, Fisher, & Becker, 2013). Flow down crustal boreholes is initiated during drilling by pumping cold (dense) seawater in the borehole adjacent to warm (less dense) formation fluid. This creates a positive differential pressure that can drive borehole fluid into the formation, even if the formation is naturally overpressured, and this flow can continue for days to years (e.g., Becker, Bartetzko, & Davis, 2001; Gable, Morin, & Becker, 1992). Downflow can be recognized from curvature of borehole temperature–depth logs and modeled based on heat balance considerations to estimate the flow rate (e.g., Becker et al., 1983; Lesem, Greytok, Marotta, & MecKetta, 1957; Winslow et al., 2013). If a natural formation overpressure exceeds the differential pressure created during downflow, the flow direction can reverse (Becker & Davis, 2004; Fisher et al., 1997). Rising borehole fluids lose heat to the formation surrounding casing, resulting in a borehole thermal profile with curvature opposite to that caused by downward flow; these flows can also be modeled to estimate the flow rate and formation properties.

Long-term borehole observatory systems (CORKs) have contributed additional data and samples related to crustal hydrogeology and alteration (e.g., Becker & Davis, 2005; Davis & Becker, 2004; Davis, Becker, Perrigrew, Carson, & MacDonald, 1992; Davis, Chapman, et al., 1992; Wheat et al., 2011). CORKs (1) seal one or more depth intervals of a borehole so that thermal, pressure, chemical, and microbiological conditions can equilibrate following the dissipation of drilling and other operational disturbances; (2) facilitate collection of fluid and microbiological samples and temperature and pressure data using autonomous samplers and data logging systems; and (3) allow long-term monitoring and large-scale active testing, including the formation response to perturbation experiments.

The CORKs developed for hydrogeologic monitoring and experiments in basement during IODP (deployed on and after Expeditions 301, 327, and 336) share features with systems deployed during earlier drilling expeditions, but have several notable differences. IODP basement CORKs are built around concentric casing strings, with the innermost casing including one or more sets of inflatable packer elements. Later IODP expeditions (327 and 336) were fitted with additional packer elements designed to expand over time through chemical interaction with seawater (Edwards et al., 2012; Fisher, Wheat, et al., 2011). Pressure measurement in these CORKs is accomplished with high-resolution

sensors and loggers, deployed on the wellhead and connected at depth using small diameter stainless steel tubing. Data from these systems are accessible using an underwater mateable connector with a submersible or remotely operated vehicle (ROV); pressure data from one IODP CORK (in Hole 1026B) are available through the Ocean Networks Canada (ONC) cabled network (http://www.oceannetworks.ca). Temperatures in most CORKs are recorded at multiple depths using autonomous sensor-logger systems that are attached to a cable suspended inside the inner CORK casing. These instruments must be recovered from the CORKs in order to download data. The CORK in Hole 1026B also provides downhole temperature data in real time through ONC.

IODP CORKs were the first designed to collect relatively pristine samples of basement fluids and microbial materials, using nonreactive casing, tubing, fittings, and coatings. Continuous Osmosampling systems were deployed with these CORKs both on the outside of seafloor wellheads (drawing samples up from below) and at depth within isolated basement intervals. Osmosampling systems were designed specifically for gas sampling (using copper tubing), microbiological incubation, tracer injection, and acid addition (Wheat et al., 2011).

In addition to providing individual monitoring and sampling points in the ocean crust, CORKs provide opportunities for active experiments and monitoring between boreholes. The experiments associated with IODP work on the eastern flank of the Juan de Fuca Ridge were designed with this as a primary project goal, and cross-hole pressure and geochemical perturbations are being used to assess crustal-scale properties and processes, including differences with depth and direction(s) of flow. Several modeling studies have also been constrained and tested using samples and data from IODP boreholes.

4.2.2.1.3 IODP Sites and Results Discussed

The locations of IODP sites discussed in this section are shown in Figure 4.2.2.1, and characteristics of selected holes are listed in Table 4.2.2.1. In several cases, boreholes started during Deep Sea Drilling Project (DSDP) or Ocean Drilling Program (ODP) operations were reoccupied (drilled, cored, and/or configured as observatories) during IODP. Figure 4.2.2.2 shows penetration depths and general lithologies of basement holes drilled during IODP, and holes drilled during DSDP and ODP having ≥100 m of basement penetration. Most sites discussed are located on the flanks of mid-ocean ridges, beyond the direct magmatic and tectonic influence of seafloor creation. Some sites are located where additional characteristics of subseafloor hydrogeology are apparent, including an exposed section of the deep crust and upper mantle near an active spreading center, crust that is about to undergo subduction, and extrusive and intrusive material associated with mid-plate volcanism. In the presentation that follows, results are introduced following the sequence of IODP *Expedition Reports*: borehole operations/configuration, lithostratigraphy, alteration, and downhole/observatory

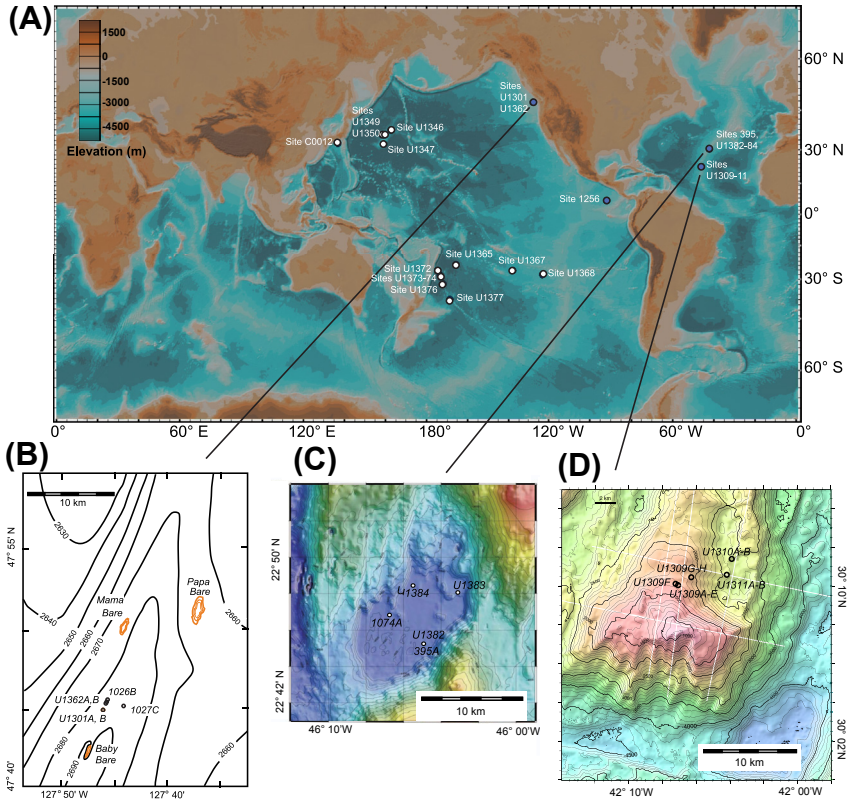

FIGURE 4.2.2.1 Black and White version: Map showing locations of drilling sites at which boreholes discussed in this chapter were created or occupied during IODP. One or more holes were drilled at each of the sites shown. Table 4.2.2.1 provides details on hole depths, lithologies encountered, and measurements made. Continental topography and ocean bathymetry are shown for reference (Ryan et al., 2009). Sites marked with open circles drilled, sampled, and/or measured basement rocks (on IODP Expeditions 322, Nankai Trough; 324, Shatsky Rise; 329, South Pacific Gyre; and 330, Louisville Seamounts), but are not discussed in this chapter. Color version: Maps showing locations of drilling sites at which boreholes discussed in this chapter were created or occupied during IODP. (A) Global map of sites with significant IODP basement penetration and analyses of hydrogeology and/or alteration. Table 4.2.2.1 provides details on hole depths, lithologies encountered, and measurements made. Continental topography and ocean bathymetry are shown for reference (Ryan et al., 2009). Sites marked with open circles drilled, sampled, and/or measured basement rocks (on IODP Expeditions 322, Nankai Trough; 324, Shatsky Rise; 329, South Pacific Gyre; and 330, Louisville Seamounts), but are not discussed in this chapter. (B) Detail map of Expedition 301/327 field area on eastern flank of Juan de Fuca Ridge *(modified from Fisher et al. (2008))*. (C) Detail map of Expedition 336 Field area in North Pond *(modified from Wheat et al. (2012))*. (D) Detail map of Expedition 304/305 field area on the Atlantis Massif *(modified from Expedition 304/305 Scientists, 2006a)*.

TABLE 4.2.2.1 Summary of Characteristics for IODP Holes with Significant Basement Penetration

Hole	Exp.	TD[a] (mbsf)	TD[a] (msb)	Core top[b] (msb)	Core bot[b] (msb)	Log top[c] (msb)	Log bot[c] (msb)	Setting[d]	Age[e] (my)
U1301A	301/321T	369.7	107.5	–	–			RF	3.5
U1301B	301/321T	582.8	317.6	86.0	317.6	86	314	RF	3.5
U1362A	327	528.0	292.0	110.0	260.0	28	271	RF	3.5
U1362B	327	359.0	117.0	–	–	–	–	RF	3.5
U1309B	304/305	101.8	99.8	0.0	99.8	20	94	RF-OCC	1.1–1.3
U1309D[f]	304/305/340T	1415.5	1413.5	18.5	1413.5	19	1413	RF-OCC	
U1310B	304/305	23.0	23.0	0.0	23.0	–	–	RF-OCC	1.1–1.3
U1311A	304/305	12.0	12.0	0.0	12.0	–	–	RF-OCC	1.1–1.3
1256D[g]	309/312/335	1521.6	1271.6	0.0	1271.6	0	1270	RF	15.0
C0012A[h]	322	576.0	38.0	0.0	38.0	–	–	RF-S	20
C0012G[h]	322	630.5	104.8	0.0	104.8	–	–	RF-S	20
U1346A[h]	324	191.8	52.6	0.0	52.6	0	58	LIP	140.0
U1347A[h]	324	317.5	159.9	0.0	159.9	0	156	LIP	145.0
U1349A[h]	324	250.4	85.3	0.0	85.3	0	84.9	LIP	140–142
U1350A[h]	324	315.8	172.7	0.0	172.7	–	–	LIP	140–142

U1365E[h]	329	124.5	53.5	0.0	53.5	–	–	RF	100.0
U1367F[h]	329	55.5	38.5	0.0	37.0	–	–	RF	33.5
U1368F[h]	329	115.1	103.3	0.0	103.3	24.2	80.2	RF	13.5
U1372A[h]	330	232.9	187.3	0.0	187.3	–	–	SM	75–77
U1373A[h]	330	65.7	31.8	0.0	31.8	–	–	SM	72–73
U1374A[h]	330	522.0	505.3	0.0	505.3	108.3	488.3	SM	72–73
U1376A[h]	330	182.8	140.9	0.0	140.9	38.1	128.1	SM	64
U1377A[h]	330	53.3	38.2	0.0	38.2	–	–	SM	50.1
U1377B[h]	330	37.0	27.9	0.0	27.9	–	–	SM	50.1
395A	336	664.0	571.0	–	–	19.0	507.0	RF	7–8
U1382A	336	210.0	120.0	20.0	120.0	8.0	120.0	RF	7–8
U1383C	336	331.5	293.2	31.2	293.2	31.2	293.2	RF	7–8

[a]TD = total depth of hole, mbsf = meters below seafloor, msb = meters subbasement, below the sediment–basement interface.
[b]Core top = depth of bit when first coring began, Core bot = depth of bit when final core ended.
[c]Log top = approximate depth of shallowest open-hole log data collected in basement, Log bot = approximate depth of deepest open hole.
[d]RF = Ridge flank, RF–OCC = Ridge flank, oceanic core complex, RF–S = Ridge flank at subduction zone, LIP = Large igneous province, SM = Seamount.
[e]Age as cited in expedition publications, generally based on magnetostratigraphy, radiometric dating, or paleontological analysis of basal sediments.
[f]Hole U1309D was drilled on IODP Expeditions 304 and 305, then revisited for additional logging on Expedition 340T.
[g]Hole1256D was first drilled, cored, and logged on ODP Leg 206.
[h]Results from drilling on IODP Expeditions 322 (Nankai Trough), 324 (Shatsky Rise), 329 (South Pacific Gyre), and 330 (Louisville Seamounts) are not discussed in this chapter, although these expeditions had significant site surveys, basement penetration, coring and downhole measurements related to crustal hydrogeology and alteration.

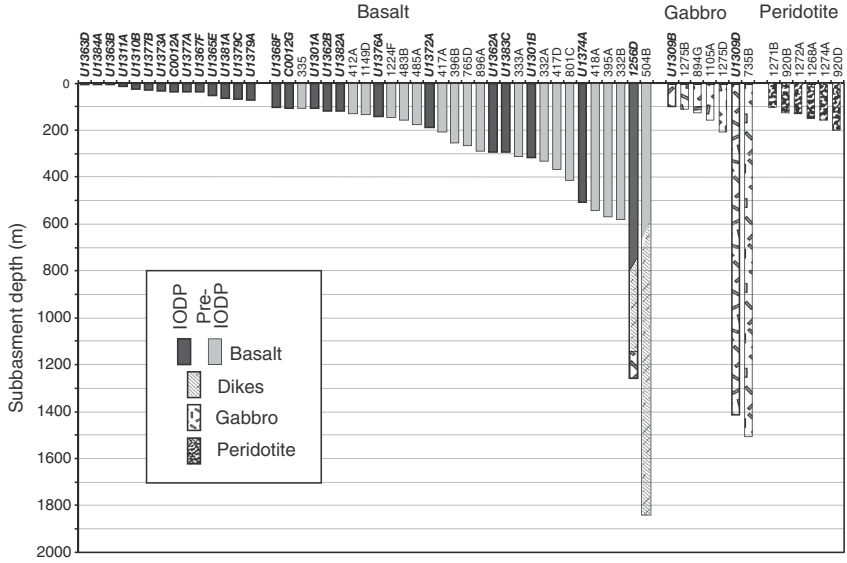

FIGURE 4.2.2.2 Plot showing total depth and general lithology for basement holes drilled during IODP (hole labels in bold italic, lithology with dark shading), and holes having ≥100 m of basement penetration from DSDP and ODP for comparison *(figure modified from Expedition 309/312 Scientists, (2006a).*). Drilling, coring, and logging intervals for most IODP basement holes are listed in Table 4.2.2.1.

measurements. Drilling and measurement depths are referenced in meters below seafloor (mbsf) and meters subbasement (msb, below the sediment-basement interface).

4.2.2.2 CRUSTAL HYDROGEOLOGY AND ALTERATION

4.2.2.2.1 Eastern Flank of the Juan De Fuca Ridge, Northeastern Pacific Ocean, ~3.5-my-old Upper Crust (IODP Expeditions 301 and 327)

4.2.2.2.1.1 Background and Context

IODP Expeditions 301 and 327 worked on the eastern end of a transect established during ODP Leg 168, on 0.9–3.6 my-old seafloor on the eastern flank of the Juan de Fuca Ridge, generated at a half-spreading rate of ~29 mm per year (Figure 4.2.2.1(B)). IODP project goals were to: resolve linked hydrogeologic, lithologic, biogeochemical, and microbiological properties and processes through analysis of sediment, rock, and fluid samples; determine the thermal, geochemical, and hydrogeologic conditions in basement; and install CORKs in the upper crust (Fisher, Tsuji, Petronotis, & the Expedition 327 Scientists, 2011; Fisher, Wheat, et al., 2011; Fisher, Urabe, Klaus, & the Expedition 301 Scientists, 2005; Fisher, Wheat, et al., 2005; Shipboard Scientific Party, 1997a). Leg

168 conducted limited basement drilling and installed two single-level CORKs in Holes 1026B and 1027C. IODP Expedition 301 researchers drilled deeper into basement at Site U1301, 1 km south of Hole 1026B; sampled sediment, basalt, and microbiological materials; logged upper basement and conducted hydrogeologic tests in Hole U1301B; replaced the borehole observatory in Hole 1026B; and established two new CORKs in Holes U1301A and U1301B. IODP Expedition 327 added two basement holes at Site U1362, between Hole 1026B and Site U1301 on the same buried basement ridge; collected sediment, rock, and microbial samples; logged upper basement and conducted hydrogeologic tests; installed two more CORKs; and recovered/replaced part of a CORK instrument string in Hole U1301B. At of the end of Expedition 327, there were six CORKs operating in this area, two completed across multiple basement depths (Holes U1301B, U1362A). Additional postdrilling expeditions have used a submersible or ROV to download data, manipulate valves, collect fluid samples, and install and recover instruments and samplers from the CORK wellheads and boreholes.

4.2.2.2.1.2 Crustal Petrology and Alteration

Basement was cored below approximately 250–265 m of sediment on Expeditions 301 and 327 in Holes U1301B and U1362A, both penetrating ~300 m into the upper volcanic crust (Table 4.2.2.1) (Expedition 301 Scientists, 2005b; Expedition 327 Scientists, 2011c). Other holes at these sites were drilled to establish borehole observatories but were not cored (U1301A and U1362B), and small amounts of basement were also recovered at Site U1363, adjacent to a seamount through which regional hydrothermal recharge occurs (Expedition 327 Scientists, 2011d). The uppermost ~100 m of basement was not cored at Sites U1301 and U1362 (Expedition 301 Scientists, 2005b; Expedition 327 Scientists, 2011c), and recovery was poor (5%) in the upper ~40 m of basement cored in nearby Hole 1026B (Shipboard Scientific Party, 1997b). Variations in drilling rates at Sites U1301 and U1362 (Becker, Fisher, & Tsuji, 2013; Expedition 301 Scientists, 2005a; Expedition 327 Scientists, 2011a) may indicate massive basalt at 55–60 msb, and breccias or highly altered pillow basalts at 65–80 msb.

Basement cores from Holes U1301B and U1362A consist mainly of pillow basalts with lesser flows, hyaloclastite breccia, and cataclastite (Expedition 301 Scientists, 2005b; Expedition 327 Scientists, 2011c). Some lava flows in both holes are >10 m thick. The basalts are normal depleted mid-ocean-ridge basalt (N-MORB), with similar trace element ratios suggesting a common magmatic source, and are aphyric to highly phyric (with olivine, clinopyroxene, and/or plagioclase phenocrysts). These basalts exhibit low-temperature alteration effects typical of upper oceanic basement (e.g., Alt, 2004), being slightly to highly altered, including a pervasive background alteration characterized by saponite (smectite clay) replacing olivine and mesostasis (Expedition 301 Scientists, 2005b; Lever et al., 2013; Ono, Keller, Rouxel, & Alt, 2012). Alteration intensities

in Hole U1301B are typically 5–25%, but can be up to 60% in brecciated intervals (Figure 4.2.2.3). Alteration is more extensive in some Hole U1362A basalts, indicative of more intensive water–rock interaction. Typical alteration features, which are more common in pillows than flows, include halos along veins and fractures, and filled veins and vesicles (with clay, celadonite, carbonate, pyrite, anhydrite and/or Fe-oxyhydroxide). The matrix of hyaloclastite and cataclastite units tends to be more highly altered than are clasts within these materials.

Oxygen isotope analyses of Hole U1301B carbonate minerals suggest temperatures of 30–40 °C during formation (Coggon et al., 2010). Secondary

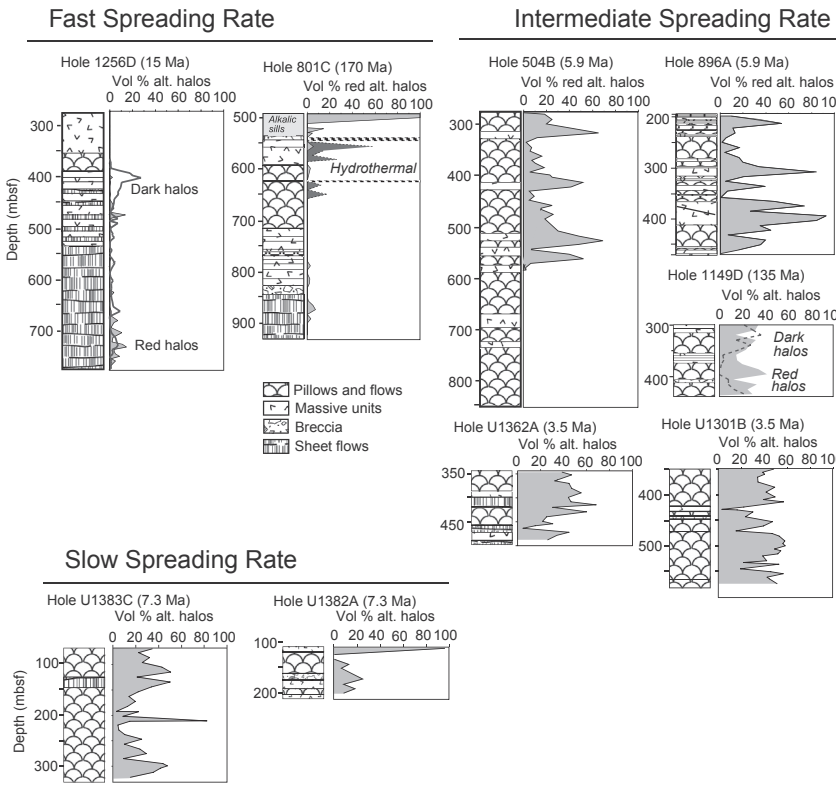

FIGURE 4.2.2.3 Lithology and proportion of alteration halos along veins versus depth for volcanic oceanic basement holes in crust grouped by fast, intermediate, and slow spreading rates. More abundant sheet flows and much lower proportion of alteration halos in crust generated at fast spreading rates may indicate control of fluid flow and low-temperature alteration by lithology and permeability (Alt et al., 2010). Hole 801C contains features not typical of the upper (generally, basaltic) oceanic crust, including a low-temperature hydrothermal deposit with associated alteration, and late alkalic sills that contain abundant alteration halos at top of basement (Alt & Teagle, 2003). Sheet flows may be more abundant than indicated (Tominaga et al., 2009). Figure modified from Alt et al. (2010), with additional data from IODP Sites U1301 (Expedition 301 Scientists, 2005b), U1362 (Expedition 327 Scientists, 2011c), and U1382 and U1383 (Expedition 336 Scientists, 2012c,d).

pyrite and bulk rocks have $\delta^{34}S$ values as low as −72‰, indicating the influence of microbial sulfate reduction in basement (Ono et al., 2012; Lever et al., 2013). These rocks also contain organic carbon with low $\delta^{13}C$ values and yield functional genes for methanogens, methane oxidizers, and sulfate reducing bacteria, providing further evidence for microbial activity in basement (Lever et al., 2013).

4.2.2.2.1.3 Geophysical Measurements and Short-term Hydrogeologic Experiments

Holes U1301B and U1362A were geophysically logged to assess borehole diameter and formation, electrical resistivity, bulk density, porosity, and sonic velocity (Expedition 301 Scientists, 2005b; Expedition 327 Scientists, 2011c). Caliper logs show oversized intervals with thicknesses of tens of meters, particularly in the upper 100–200 msb, and more massive formation conditions at greater depth. In general, oversized zones correspond to lithologies of pillow basalt, breccia, and hyaloclastite, but core recovery within these intervals is typically low, so correlating lithology and alteration with geophysical response in these intervals is challenging.

Bulk density logs include zones 1–10-m thick having values of 2900–3000 kg/m^3, consistent with measurements made on core samples (Bartetzko & Fisher, 2008; Becker et al., 2013). There are also thin zones within both boreholes that have bulk density of 1800–2200 kg/m^3 and are not oversized, suggesting more fractured and/or porous conditions. In general, pillow basalts tend to have more of these low-density intervals than do other lithologies.

Hydrogeologic tests were run in Holes U1301B and U1362A with a drillstring packer (Becker & Fisher, 2008; Becker et al., 2013), with the packer set where basement rocks were relatively massive and the hole diameter could support the inflated packer element. The deepest packer setting depth in Hole U1301B corresponds to an abrupt change in the character of basement geophysical logs (near 470 mbsf, 205 msb), with more variable borehole diameter and physical properties (bulk density, resistivity, sonic velocity) at shallower depths. Below this depth, logs indicate more massive conditions, but there are thin zones of lower density that could be brecciated or fractured (Bartetzko & Fisher, 2008; Expedition 301 Scientists, 2005b).

Packer tests of the interval below 472 mbsf (207 msb) in Hole U1301B indicate bulk permeability of $k = 1.7 \times 10^{-12}$ m^2, whereas tests with the packer at 442 and 417 mbsf (177 and 152 msb, respectively) indicate higher permeability, $k = 3.2 \times 10^{-12}$ m^2. If the properties determined at shallower setting depths are applied to the uppermost ~200 m of basement, permeability within this interval is closer to $k = 5 \times 10^{-12}$ m^2. The consistency of properties determined with two shallow setting depths suggests that most of the formation transmissivity may be concentrated between ~150 and 180 msb; if so, the bulk permeability of this 30-*m*-thick zone would be $k = 2 \times 10^{-11}$ m^2 (Becker & Fisher, 2008).

The single-packer setting depth in Hole U1362A was near 190 msb, within a 20-*m*-thick massive zone that separates two oversized zones (Becker et al., 2013). Results from these tests indicate bulk permeability of $k = 1–2 \times 10^{-12}$ m^2, essentially the same as determined at the deepest setting depth in Hole U1301B, 825 m to the south. Bulk permeability values deeper than ~150 msb in both holes are higher by roughly an order of magnitude than those obtained by Becker and Fisher (2000) in the shallowest basement sections in nearby Holes 1026B and 1027C. This suggests considerable heterogeneity and/or that the highest upper crustal permeabilities in this area are not located immediately adjacent to the sediment–basement interface, but are deeper in the extrusive section (Becker & Fisher, 2008; Becker et al., 2013; Fisher, Davis, & Becker, 2008).

4.2.2.2.1.4 Long-term Observatory Measurements and Samples

Single-level CORKs were installed in Holes 1026B, U1301A and U1362B, and two-level CORKs were installed in Holes U1301B and U1362A (Fisher, Wheat, et al., 2011; Fisher, Wheat, et al., 2005). The CORKs installed in Holes U1301A and U1301B were not sealed as intended during deployment. Incomplete sealing and the imposition of a cold column of water in the boreholes during drilling, casing, and other operations led to self-sustained flow of cold ocean-bottom water down these holes and into the formation. The Hole U1301B CORK was partly sealed in Summer 2007 with cement deployed by submersible, and was fully sealed in Summer 2009 by cementing with the drillship, stopping the downflow of cold bottom water after 5 years (Expedition 327 Scientists, 2011b; Fisher, 2010). The Hole 1301A CORK was also cemented with the drillship in Summer 2009, but much of that cement drained away within a few hours to days, so that CORK has remained unsealed. However, the downflow into Hole 1301A that began in 2004 when the hole was drilled, varied in rate and slowed over several years, then reversed abruptly in September 2007 (Wheat et al., 2010). Since this time, Hole U1301A has been a site of warm (~64 °C) hydrothermal discharge. Interestingly, the geochemistry of fluids discharging from Hole U1301A showed little evidence for recharge of bottom water in nearby Hole U1301B, only 36 m away, even before Hole U1301B was cemented. This observation provides evidence for separation (heterogeneity) of flow systems within the upper oceanic crust.

The CORK in Hole 1027C was supposed to be replaced during Expedition 327, but the old CORK could not be removed. Instead, the Hole 1027C CORK was modified a year later using an ROV by recovering the old data logger and installing a pressure monitoring manifold and a new data logger (Fisher et al., 2012). The other five CORKs installed in this area are installed above a buried basement high, along a transect 1-km-long that is oriented parallel to the active spreading center and the trend of abyssal hill topography. Hole 1027C is located about 2.4 km to the east, above a thicker sediment section where the top of basement is >300 m deeper below the seafloor.

Pressure records recovered from these CORKs show that upper basement is overpressured at Sites 1301 and 1362 by tens of kilopascals with respect to an ambient hydrostatic column, and the upper basement interval monitored in Hole 1027C is underpressured by tens of kilopascals, consistent with earlier measurements (Davis & Becker, 2004; Davis, LaBonte, He, Becker, & Fisher, 2010). Pressure data recovered from Hole 1362A, which monitors two distinct basement intervals, show that the overpressure is greater with greater depth in the hole, consistent with net upward transport of fluid below the buried basement high, as inferred from coupled fluid-heat modeling (Spinelli & Fisher, 2004).

Temperature loggers were recovered from near the top of basement in CORKs in Holes U1301A and U1301B in 2009 (by submersible) and 2010 (by drillship), respectively, following 4–5 years of deployment (Expedition 327 Scientists, 2011b; Wheat et al., 2010). These loggers recorded thermal conditions during a long period of fluid downflow. These thermal data and additional information (borehole geometry, completion details, and basement stratigraphy) were used to assess upper basement hydrogeologic properties with linked analytical models and a statistical analysis using a range of borehole parameters (Winslow et al., 2013). These analyses suggest that the initial flow rate down Hole U1301A (before flow reversal) was ~2 L/s, whereas ~20 L/s flowed down Hole U1301B. Flow may have been more rapid down Hole U1301B, compared to Hole U1301A, because Hole U1301B extends deeper into basement (which imposes a taller column of cold, dense bottom water), and because the formation permeability around Hole U1301B appears to be somewhat greater (Winslow et al., 2013).

Wheat et al. (2010) evaluated the thermal and geochemical response of Hole 1301A before, during, and after the reversal from downflow to upflow. In addition to a thermal response associated with changes in flow rate and direction, two single-hole tracer experiments elucidate the geochemical composition and nature of mixing of borehole and formation fluids. Osmosamplers deployed within slotted casing near the base of the CORK, surrounded by basaltic upper crust, collected fluids throughout the deployment. Major ion chemistry shows relatively consistent concentrations of solutes such as Mg, close to bottom water values, until the flow reversal occurred. After the flow reversal, when reacted crustal fluid flowed rapidly from the formation into and up the borehole, the sampled fluid composition was similar to that seen in fluids sampled from nearby Baby Bare outcrop and ODP Hole 1026B (Shipboard Scientific Party, 1997b; Wheat et al., 2010, 2004). One of the Osmosampler packages deployed in Hole U1301A also injected a tracer solution (containing Cs, Yb, and Tm). Evaluation of tracer concentrations in sampled fluids suggests that the rates of mixing and flow resulted in a volume exchange rate for the sampled interval of ~60% per week during the initially rapid period of downflow, 1–15% per week during the slowdown in downflow that preceded reversal, and ~99% per week after upflow of formation fluids began in 2007 (Wheat et al., 2010).

A large-scale assessment of basement hydrogeologic properties was made from the long-term pressure perturbation observed in Hole 1027B that resulted from leakage of cold bottom seawater into the crust around Hole U1301B following Expedition 301 (Fisher et al., 2008). Both IODP Expedition 301 basement operations and subsequent downflow into the crust influenced pressures in sealed Hole 1027C. Although basement operations in Hole U1301B caused a direct pressure response in Hole 1027C, operations in nearby Holes U1301A and 1026B had little or no influence. The packer experiments in Hole U1301B caused the greatest immediate perturbation, despite modest pumping rates, because fluids injected during this test were forced to enter basement below the seal by the packer element, rather than being allowed to flow back up the borehole to the overlying ocean. These observations suggest that shallow basement surrounding Holes U1301A and 1026B may be less well connected hydrologically to the uppermost oceanic crust around Hole 1027C than is deeper basement in Hole U1301B.

A comparison of pressure conditions in these holes, and correlation with drillship and later borehole operations, suggest a flow rate into Hole U1301B during the 13 months following Expedition 301 of Q = 2–5 L/s (Fisher et al., 2008). This flow rate and the observed 13-month pressure change in Hole 1027C (~1.5 kPa in total) suggest a bulk basement permeability of $k = 0.7–2 \times 10^{-12}$ m^2 (Figure 4.2.2.4). This inadvertent cross-hole experiment provided a direct measurement of the storativity of the upper volcanic crust, a term that depends on a combination of crustal and fluid compressibility, and cannot be determined with single-hole pumping experiments. Upper crustal compressibility was calculated to be $\alpha = \sim 3$ to 9×10^{-10} Pa^{-1}, close to or somewhat greater than that of seawater under ambient thermal and pressure conditions. Davis et al. (2010) completed additional analyses of the cross-hole response between Sites 1301 and 1027C, and explored the properties required to sustain downflow into an open basement hole. Their analytical and numerical calculations indicate a minimum basement permeability of $k = 3–4 \times 10^{-13}$ m^2, consistent with earlier analytical calculations. Modeling also showed how the time required for a flow reversal (if one occurs) depends on formation permeability and the depth of the flowing borehole.

These CORKs were most recently serviced in Summer 2014, with downhole samplers and data loggers recovered from Holes 1026B, U1362A, and U1362B, and data and samples collected from wellhead instruments in these CORKs and those in Holes 1301A and 1027C. Data and samples analyzed to date show clear evidence for cross-hole pressure perturbations associated with the long-term flow experiment, and the arrival of tracers in multiple holes distant from that used for tracer injection on Expedition 327, Hole U1362B.

4.2.2.2.1.5 Hydrogeologic Modeling

Numerical models were used to calculate hydrologic properties consistent with inferred rates of fluid circulation between Grizzly Bare and Baby Bare outcrops, which are recharge and discharge sites separated by 50 km (south and north of the Expedition 301/327 work area, respectively) (Hutnak et al., 2006).

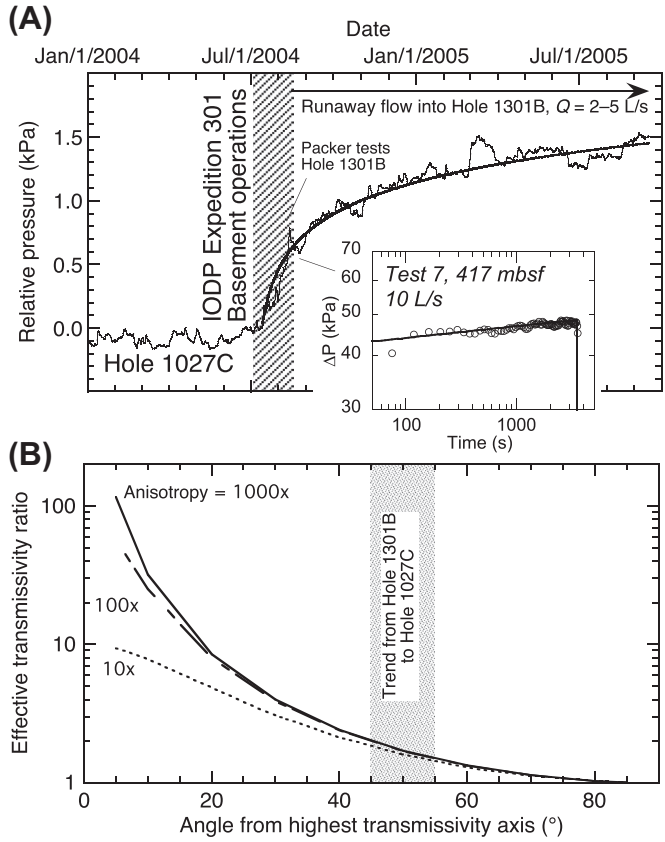

FIGURE 4.2.2.4 Data from hydrogeologic experiments in the IODP Expedition 301/327 field area *(plots modified from Becker & Fisher (2008) and Fisher et al. (2008))*. A. Observations and calculations from cross-hole test. (A) Filtered pressure-time record from Hole 1027C, beginning 6 months before and ending 13 months after Expedition 301. Striped vertical band indicates period of basement drilling, coring, casing, and testing operations during Expedition 301. Smooth curve shows least squares best fit of observations to analytical calculations for the pressure response in Hole 1027C, 2.4 km away, to long-term flow into Hole U1301B. The fit of this curve indicates basement permeability of $k = 0.7–2 \times 10^{-12}$ m^2. Inset: Similar fit to short-term (1-h) packer experiment in Hole 1301B, illustrating fit of the same model, but using a basement permeability of 3×10^{-12} m^2. Note relatively large change in pressure during this test (up to 50 kPa) versus that seen from the cross-hole response (~1.5 kPa). (B) Calculations of the effective transmissivity ratio (apparent transmissivity/highest transmissivity) as a function of the angle of measurement between the dominant transmissivity direction and the direction of measurement. Vertical band is orientation of the Site U1301 to Site 1027 experiment, assuming that the direction of highest transmissivity is N20°E (subparallel to the crustal fabric) and the direction of lowest transmissivity is perpendicular to this, N110°E. For essentially any transmissivity anisotropy ratio, the value measured between Sites U1301 and 1027C will be close to that for the lowest transmissivity direction.

This work followed analytical calculations of basement permeability needed to maintain a self-sustaining, hydrothermal siphon (Fisher, Davis, et al., 2003). Two-dimensional, transient numerical models suggest that outcrop-to-outcrop circulation can be sustained across this distance when basement permeability between outcrops is $\geq 10^{-12}$ m^2 (Hutnak et al., 2006). At lower permeabilities, too much energy is lost during lateral fluid transport for circulation to continue without forcing, given the limited driving pressure difference at the base of recharging and discharging fluid columns in the crust.

These models also showed that fluid temperatures in upper basement are highly sensitive to modeled permeability. Observed upper basement temperatures in this area are generally 60–65 °C (Davis, Chapman, et al., 1992; Expedition 301 Scientists, 2005b; Hutnak et al., 2006; Shipboard Scientific Party, 1997b), about the same as would result from fully conductive conditions. This means that, whatever the flow rate between Grizzly Bare and Baby Bare outcrops (and across Sites U1301 and U1362), there is little advective heat extraction on a regional basis. Modeling showed that when crustal permeability is too high ($\geq 10^{-10}$ m^2), fluid circulation between outcrops is so rapid that basement is chilled to temperatures well below those observed (modeled values of 20–50 °C). A better match to observed upper basement temperatures of 60–65 °C is achieved when lateral basement permeability is ~10^{-11} m^2 (Hutnak et al., 2006).

Additional models were crafted to assess the significance of "background" heat flow around the Expedition 301/327 work area. Thermal data collected during regional studies showed that heat flow along a 100-km-long swath of 3.4–3.6-my-old seafloor is lower by 15–20% than predicted by conductive lithospheric cooling models, even after correcting for rapid sedimentation rates (an additional 12–18% correction) (Davis et al., 1999; Hutnak et al., 2006; Zühlsdorff et al., 2005). Observations show no regional recharge-to-discharge trend in heat flow (e.g., Langseth & Herman, 1981; Stein & Fisher, 2003), and no low-heat flow "moat" around Grizzly Bare outcrop (Hutnak et al., 2006; Zühlsdorff et al., 2005), as might be expected if present-day fluid flow were responsible for the regional anomaly.

Calculations show that the Expedition 301/327 work area (and much of the surrounding region) could be undergoing "thermal rebound" following the cessation of a long period of more efficient, advective heat extraction from the crust (Hutnak & Fisher, 2007). Maps of basement relief and sediment thickness in this area show numerous shallowly buried basement highs (Hutnak et al., 2006; Zühlsdorff et al., 2005); basement in many of these areas would have been exposed at the seafloor prior to the last several hundred thousand years of rapid sedimentation, and areas of current basement exposure (e.g., Baby Bare outcrop) would have been larger and better connected to the ocean (Hutnak & Fisher, 2007). Larger areas of basement exposure, and the greater spatial distribution of these areas, would have been permitted more efficient regional advective heat loss, as is currently seen at the western end of the Leg 168 transect (Davis, Chapman, et al., 1992; Hutnak et al., 2006), where measured heat flow

is ~20% of lithospheric predictions, and on other ridge flanks where basement outcrops are more common (e.g., Hutnak et al., 2008; Lucazeau et al., 2006; Villinger, Grevemeyer, Kaul, Hauschild, & Pfender, 2002).

4.2.2.2.2 Western Flank of the Mid-Atlantic Ridge, Northern Atlantic Ocean, 7.3-my-old Upper Crust (IODP Expedition 336)

4.2.2.2.2.1 Background and Context

IODP Expedition 336 was designed to explore the subseafloor biosphere, geology, geochemistry, and hydrogeology at a young ridge-flank site known as North Pond (Figure 4.2.2.1(C)). The ocean crust in this area was created at the Mid-Atlantic Ridge (MAR) at a half-spreading rate of 14 mm per year. In contrast to the Expedition 301/327 work area, the seafloor around North Pond is characterized by patchy sediment cover and extensive basement exposure. Rapid fluid flow is thought to occur in the volcanic crust below North Pond, limiting upper basement temperatures to ≤20 °C (Langseth, Becker, Von Herzen, & Schultheiss, 1992; Langseth, Hyndman, Becker, Hickman, & Salisbury, 1984). Site 395 was first drilled during DSDP Leg 45 (Shipboard Scientific Party, 1979) and has been revisited multiple times for logging, hydrogeological studies, and other survey work (mapping, seismics, shallow coring, and heat flow) (e.g., Becker et al., 2001; Becker, Langseth, & Hyndman, 1984; Morin, Hess, & Becker, 1992; Morin, Moos, & Hess, 1992). Processes and conditions at North Pond are likely to be typical of ridge-flank hydrothermal circulation through young crust in many settings: rapid flow of cool fluids having limited opportunity to react with basement rocks and overlying sediments before being discharged to the overlying ocean. Samples and data collected during a site survey prior to Exp. 336 are consistent with this interpretation (Ziebis et al., 2012).

The principal objectives of IODP Expedition 336 to North Pond were addressed through coring and analyses of recovered materials, borehole geophysical and fluorescence measurements, and use of CORKs for monitoring and sampling after drilling was complete (Expedition 336 Scientists, 2012a). Basement was cored in two holes on Expedition 336 discussed in this section: Hole U1382A and Hole U1383C (Table 4.2.2.1).

4.2.2.2.2.2 Crustal Petrology and Alteration

Basement coring at Hole 395A recovered mainly pillows and massive basalt units (Shipboard Scientific Party, 1979). The pillow units are typically tens of meters thick and separated by a sedimentary breccia unit that contains cobbles of gabbro and serpentinized peridotite derived from the surrounding basement peaks (Bartetzko, Pezard, Goldberg, Sun, & Becker, 2001; Matthews, Salisbury, & Hyndman, 1984). Nearby Hole 395 also contains a peridotite–gabbro complex that is several meters thick with brecciated contacts (Shipboard Scientific

Party, 1979). Oxygen isotope data for carbonate and clay veins in the volcanic basement from these holes are consistent with low temperatures, around 30 °C for phyllosilicates and 0–15 °C for carbonates (Lawrence & Gieskes, 1981).

Basement cores recovered from Hole U1382A suggest that pillow lavas are slightly more abundant than massive lavas (32% recovery) (Expedition 336 Scientists, 2012c). Fragments of hyaloclastite are present in a few pillow units, and there is sedimentary breccia that contains clasts of gabbroic rocks and weakly serpentinized harzburgite and lherzolite. This breccia likely represents a rockslide deposit and was also encountered in Holes 395 and 395A, within 80 m of Hole U1382A. The full lateral extent of this lithological unit and its influence on the upper basement transmissivity are not known. The basalts are aphyric to highly plagioclase-olivine phyric, are all N-MORB, but have variable immobile trace element ratios (Zr/Y and Ti/Zr) indicative of distinct parental magmas.

Hole U1382A basalts show evidence for low-temperature alteration by seawater: pervasive clay background alteration and common halos around veins, comprising approximately 15–20% of the recovered core (Expedition 336 Scientists, 2012c). Phyllosilicates (smectite > celadonite) are the most abundant secondary phases, followed by Fe-oxyhydroxides and minor zeolites and carbonates. Veins are abundant (13–20 veins/m) but narrow (usually <0.2 mm in width). Common carbonate-filled vein networks are associated with intense oxidative alteration of olivine to clay, oxide, and carbonate (Expedition 336 Scientists, 2012c).

Basalt samples recovered from Hole U1383C feature a greater proportion of thin flows with glassy margins, leading to more extensive palagonitization and greater vein density (33 veins/m) (Expedition 336 Scientists, 2012d). Background alteration of the basalts is ≤40% in the shallower sections and decreases downhole (Figure 4.2.2.3). Vesicle fills of clay, phillipsite, calcium carbonate, and Fe-oxyhydroxide are common. Around 20% of the recovered core consists of brownish alteration halos that flank veins. Veins fills are dominantly clay and Fe-oxyhydroxide with only minor carbonate in the uppermost 150 m of basement. The lowermost 100 m of Hole U1383C feature mixed zeolite/carbonate veins with variable, but usually small, proportions of clay. Veins are more common in this deeper section, but background alteration is less pronounced than in uppermost basement (Expedition 336 Scientists, 2012d).

4.2.2.2.2.3 Geophysical Measurements

Wireline logging in Hole 395A during Expedition 336 included natural gamma ray, temperature, and induced fluorescence to identify microbial material ("DEBI-t" tool) (Expedition 336 Scientists, 2012b). Natural gamma ray and resistivity data are consistent with results from earlier logging (e.g., Bartetzko et al., 2001; Matthews et al., 1984; Moos, 1990), defining individual eruptive and flow units. The upper 300 m of basement comprises lithologic units having thicknesses of approximately 10–70 m, within which there is generally a bottom-to-top decrease in electrical resistivity, bulk density, and compressional velocity, and an increase in natural gamma ray emissions. Some of these units are separated by thinner

(1–10 m) layers of breccia, altered flows, or massive basalt. Fluorescence data from the DEBI-t tool suggests elevated photon counts at several wavelengths, particularly at 455 nm, in the upper 100 msb. The excitation source (224 nm) is intended to give peak fluorescence responses near 300 nm for spores and 320 nm for bacteria, but variations in depth with these wavelengths are not as clear as those at 455 nm (Expedition 336 Scientists, 2012b).

The upper 100–300 msb were logged in Holes U1382A and 1383C with caliper, natural gamma ray, bulk density, and resistivity tools, revealing lithologic layering at a scale of 5–20 m, but without the systematic delineation of individual eruptive units apparent in Hole 395A (Expedition 336 Scientists, 2012c; d). Geophysical logging units defined on the basis of log response are finer than those identified from recovered core (≤30%) (Expedition 336 Scientists, 2012d). Also in contrast to results from Hole 395, logging in these holes revealed no trends in downhole fluorescence (Expedition 336 Scientists, 2012c).

4.2.2.2.2.4 Long-term Observatory Measurements and Samples

Expedition 336 CORKs included multiple nested casing strings and packer systems (inflateable and swellable), casing seals, and nonreactive components deployed at depth (Edwards et al., 2012). Expedition 336 CORKs were the first to use fiberglass inner casing, along with resin-coated steel casing and collars introduced in earlier CORKs, in an effort to allow collection of near-pristine samples of basement fluids and microbial materials. Downhole pressure, temperature, and dissolved oxygen are being monitored for short-term and long-term variability, and downhole and wellhead sampling systems are collecting fluids at a range of rates in different storage media, and providing substrate for microbial incubation. A single-level CORK was deployed in Hole U1382A to monitor conditions in the upper 120 m of volcanic crust (Expedition 336 Scientists, 2012c), and three-level CORKs were deployed in Holes 395A (after removal of an old borehole observatory) and U1383C (Expedition 336 Scientists, 2012b,d). Hole U1382B was drilled and cased during Expedition 336, then left open for later instrumentation using a "CORK-lite" system deployed with a remotely operated vehicle (Expedition 336 Scientists, 2012c; Wheat et al., 2012). Data and samples from these systems will inform understanding of hydrogeologic, geochemical, and microbiological conditions in basement below and around North Pond in coming years.

4.2.2.2.3 Eastern Flank of the East Pacific Rise, Eastern Pacific Ocean, ~15-my-old Upper to Middle Crust (IODP Expeditions 309, 312, and 335)

4.2.2.2.3.1 Background and Context

Site 1256 was drilled to test models for the structure and origin of seismic layering of oceanic crust and the origin of melt lenses at fast-spreading ridges, in 15-my-old crust that formed at a superfast spreading rate (half rate

~100 mm per year) at the East Pacific Rise (EPR) (Expedition 309/312 Scientists, 2006b; Expedition 335 Scientists, 2012; Shipboard Scientific Party, 2003). Drilling, coring, and measurements were initiated on ODP Leg 206 and continued on IODP Expeditions 309, 312, and 335. Coring in Hole 1256D started at 276 mbsf (26 msb) and ended at 1522 mbsf (1246 msb) (Expedition 309/312 Scientists, 2006b; Expedition 335 Scientists, 2012; Shipboard Scientific Party, 2003). Hole 1256D is currently the fourth deepest penetration into oceanic basement, extending through lavas, dikes, and into gabbros (Figure 4.2.2.2).

4.2.2.2.3.2 Crustal Petrology and Alteration

The uppermost basement in Hole 1256D comprises a ~100-m-thick sequence dominated by a ponded flow >75-m thick; the same massive flow is only 32-m thick in nearby Hole 1256C (Expedition 309/312 Scientists, 2006b). The immediately underlying lavas include sheet and massive flows and minor pillow flows. The amount of basement relief indicated by variation in the thickness of the ponded flow, and the presence of flow lobe inflation features, indicate that the upper 284 m of the volcanic section crystallized off-axis (Expedition 309/312 Scientists, 2006b; Tominaga, Teagle, Alt, & Umino, 2009). Sheet flows and massive lavas erupted at the ridge axis, and two thin (1–2 m) hyaloclastite intervals (at 397 and 595 mbsf) make up the remaining extrusive section (Figure 4.2.2.5). The beginning of a lithologic transition at 1004 mbsf is marked by subvertical intrusive dike contacts and sulfide-mineralized breccias. Below 1061 mbsf, subvertical intrusive contacts indicate a ~350-*m*-thick sheeted dike complex, with the lowermost ~60 m characterized by recrystallization to granoblastic textures by contact metamorphism.

The plutonic complex begins at 1407 mbsf (Figure 4.2.2.5), and consists of a 52-m-thick upper gabbro, a 24-m-thick interval of recrystallized granoblastic dikes with minor gabbroic and felsic veins, and a 24-m-thick lower gabbro. Contacts of the gabbros with the intervening dike interval are intrusive, with partly resorbed, stoped dike clasts within the gabbros. The plutonic section has been interpreted as either two separate gabbro units intrusive into the sheeted dikes, with an intervening screen of dikes (Expedition 309/312 Scientists, 2006b; Koepke et al., 2008); or as a single lens of gabbro containing stoped dike clasts, with the poorly recovered intermediate dike interval representing stoped dike fragments within gabbro (France, Ildefonse, & Koepke, 2009; Koepke et al., 2011).

Flows and dikes are aphyic to sparsely phyric and variably fractionated, with MgO contents of approximately 10–4.5 wt% (Expedition 309/312 Scientists, 2006b; Shipboard Scientific Party, 2003). The ranges of most major and many minor element concentrations are similar to those of the northern EPR, suggesting processes analogous to those along the modern EPR. Gabbro compositions are similar to the flows and dikes, but are on average more primitive, with higher MgO numbers (Expedition 309/312 Scientists, 2006b; Koepke et al., 2011).

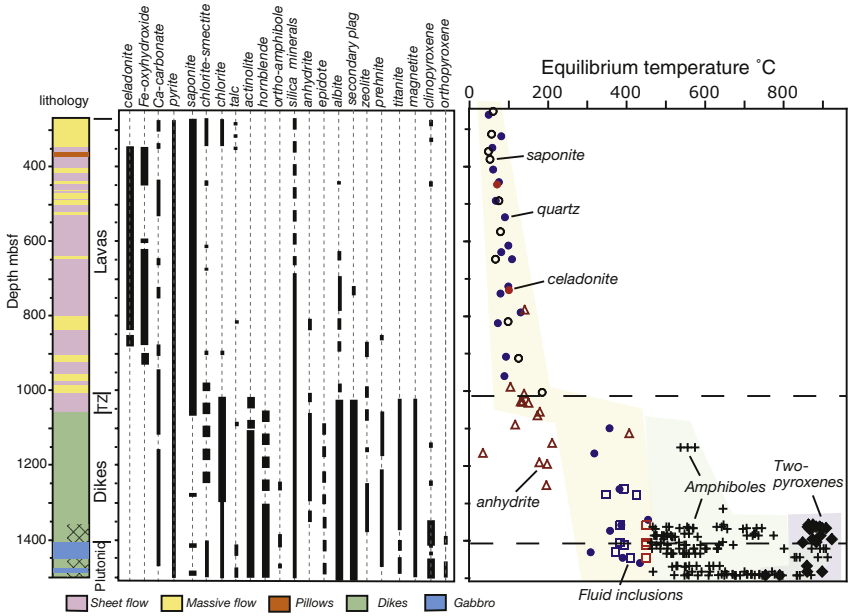

FIGURE 4.2.2.5 Basement lithology, distribution of secondary minerals, and estimated alteration temperatures for Hole 1256D *(modified from Alt et al. (2010))*. Figure illustrates stepped temperature gradient with depth. Secondary minerals and temperature estimates indicate low-temperature seawater fluids in the volcanic section and upwelling high-temperature hydrothermal fluids in the dikes. Stepwise temperature increase at lavas–dikes transition results from mixing of these fluids at this lithologic boundary. Stepwise increase at ~1350 mbsf indicates heating and contact metamorphism of lowermost dikes from underlying gabbroic intrusion. Range of temperatures in plutonic and dike sections results from retrograde reaction during cooling. Temperatures estimated from oxygen isotope analyses of secondary minerals, mineral equilibria, and fluid inclusions.

Hole 1256D sampled the transition between low-temperature and high-temperature hydrothermal alteration in a continuous section of oceanic crust (Alt et al., 2010) (Figure 4.2.2.5). Extrusives exhibit typical low-temperature alteration, with a pervasive saponitic (clay) background alteration, with dark and brownish alteration halos that contain celadonite (mica) and Fe-oxyhydroxide along veins. This vein-related alteration is concentrated in two zones, at 350–450 and 635–750 mbsf (Figure 4.2.2.3). Veins average 30/m, and vein minerals include saponite, Fe-oxyhydroxide, celadonite minor pyrite, and rare carbonate. Alteration temperatures in the lavas, estimated from oxygen isotope analyses of secondary minerals, were approximately 50–125 °C, generally increasing downward (Alt et al., 2010). Sulfur isotope data indicate widespread effects of microbial sulfate reduction in the volcanic sequence (Alt and Shanks, 2011), as in other oceanic basement sections (Lever et al., 2013; Ono et al., 2012; Rouxel, Shanks, Bach, & Edwards, 2008). The basal lava section features intervals with pyrite-rich alteration halos, mixed-layer chlorite-smectite, and anhydrite, and

oxygen isotope analyses of secondary minerals indicate higher temperatures (150°–200 °C) than shallower in the crust (Alt et al., 2010).

The appearance of chlorite, albite, actinolite, anhydrite, epidote, and laumontite at around 1000 mbsf and the presence of an intensely altered and mineralized hyaloclastite breccia at 1022 mbsf indicate a stepwise increase in alteration temperatures downward across the top of the transition from lavas to dikes, and reaction with high-temperature hydrothermal fluids (Figure 4.2.2.5). Rocks are typically more intensely altered in centimeter-scale halos along veins in the dike margin breccias. Circulating hydrothermal fluids had temperatures (approximately 320–450 °C), salinities, and oxygen isotope compositions similar to black smoker fluids (Alt et al., 2010). Chlorite is the most common vein filling in the dikes, but quartz, sulfide, actinolite, prehnite, laumontite, and calcite are also present, and anhydrite veins are common to ~1200 mbsf. Hydrothermal veins composed of quartz, epidote, and sulfide postdate the chlorite-dominated veins, and are crosscut by vein assemblages of anhydrite, prehnite, laumontite, and calcite (formed <250 °C). Alteration mineralogy below ~1350 mbsf indicates temperatures >480 °C. In the lower portion of the sheeted dikes (1370–1397 mbsf), the rocks are recrystallized in patches to granoblastic textures, with secondary clinopyroxene, orthopyroxene, actinolitic hornblende, plagioclase, and blebs of oxide (ilmenite and magnetite). The pyroxene-rich assemblage and the granoblastic textures indicate recrystallization of previously hydrothermally altered rocks at temperatures >800 °C, related to underlying gabbroic intrusions (Alt et al., 2010; Koepke et al., 2008).

The plutonic section comprises highly altered gabbro and felsic veins with amphibole, chlorite, plagioclase, titanite, and minor laumontite and epidote, with alteration temperatures and hydrothermal fluid compositions similar to those in the overlying lower dikes. The dike screen separating the two gabbro units is recrystallized to granoblastic textures at temperatures similar to those in the basal granoblastic sheeted dikes. The intensity of gabbro alteration is variable, with intrusive margins and dike screen contacts being most extensively hydrothermal altered (Teagle & Wilson, 2007).

The overall alteration scenario involves cooler seawater fluids circulating in the volcanic section, and high-temperature hydrothermal fluids in the underlying dikes and gabbros. The stepwise increase in temperature downward across the top of the lava–dike transition (Figure 4.2.2.5) and the presence of a mineralized breccia indicate a mixing zone between these two fluid and alteration regimes (Alt et al., 2010). Evidence for black smoker-like fluid compositions and the presence of mineralized dike margins at greater depths indicate upwelling hydrothermal fluids in the dike section. Variations in profiles of oxygen and lithium isotopes result from these thermal regimes and compositional variations within the dikes (Gao et al., 2012). Contact metamorphism of the lowermost hydrothermally altered dikes resulted in a second thermal step at this depth, which decayed as the section cooled back to hydrothermal conditions (Alt et al., 2010).

4.2.2.2.3.3 Geophysical Measurements

Borehole geophysical logs collected in Hole 1256D during IODP Expeditions 309, 312, and 335 included natural gamma ray, bulk density, porosity, sonic velocity, electrical resistivity, temperature, and borehole imaging instruments (Expedition 309/312 Scientists, 2006b; Expedition 335 Scientists, 2012).

Wireline logs from the upper crust show variable borehole diameter, particularly within the interval 350–460 mbsf (100–210 msb), with corresponding decreases in electrical resistivity, bulk density, and sonic velocity, and increases in neutron porosity. These correlations could indicate that local anomalies result in part from poor borehole conditions, but the elevated natural gamma ray values suggest that there may be more extensive alteration in the inflated flows of this interval. The overlying, more massive, lava pond interval generally shows lower natural gamma radioactivity, and higher resistivity, bulk density, and sonic velocity, despite the relatively large borehole diameter. There are additional zones of elevated natural gamma ray emissions within the basalt sheets and massive flows between 780 and 900 mbsf (530–650 msb), despite having a borehole diameter that is mostly to gauge. Borehole imaging provides clear views of formation lithologic changes, for example, showing thin flow and pillow shapes in the upper volcanic crust, and allows assessment of fracture occurrence and orientation (Expedition 309/312 Scientists, 2006b; Expedition 335 Scientists, 2012). Core samples from Hole 1256D down to ~1000 msb yielded *P*-wave velocity values that are consistent with both wireline borehole logs and a vertical seismic profile experiment, indicating a lack of large-scale porosity (fractures) (Swift, Reichow, Tikku, Tominaga, & Gilbert, 2008). Below this depth, wireline logs indicate velocities higher than those measured with core samples, which may indicate a stress response associated with unloading of samples during coring and recovery (Expedition 309/312 Scientists, 2006b).

Thermal measurements indicate that borehole conditions were conductive prior to drilling and that heat flow through the basement section is essentially the same as that determined for the overlying sediments (Expedition 309/312 Scientists, 2006b; Shipboard Scientific Party, 2003). The lack of curvature in the temperature profile through the cased sedimentary section suggests that there is little or no fluid flow down the borehole, despite imposition of a cold column of fluid during drilling and other operations. Heat flow determined during drilling of the sedimentary section at this site, 113 mW/m^2, is close to the 120–130 mW/m^2 predicted by standard lithospheric cooling curves for seafloor that is 15-my old. This is unusual in comparison to the global heat flow data set for seafloor of this age, which typically shows evidence for advective extraction of ~40% of lithospheric heat (e.g., Stein, Stein, & Pelayo, 1995). Collectively these results suggest that the basement rocks around Hole U1256D may not currently be as hydrothermally active as is common for crust of this age.

4.2.2.2.4 Adjacent to the MAR and Atlantis Transform Fault, Northern Atlantic Ocean, Approximately 1.1–1.3-my-old Upper and Lower Crust (IODP Expeditions 304 and 305)

4.2.2.2.4.1 Background and Context

Expeditions 304 and 305 explored an oceanic core complex at the Atlantis Massif on the young western flank of the MAR at 30°N (Expedition 304/305 Scientists, 2006a) (Figure 4.2.2.1(D)). Exposure of gabbroic and mantle rocks along slow-spreading ridges is common (Escartín et al., 1998), and Exp. 304/305 researchers sought to understand mechanisms of lithospheric accretion by detachment faulting, at a site where the spreading half rate is ~12 mm per year. The "corrugated" central part of the Atlantis Massif is inferred to have been formed by detachment faulting during or soon after crustal formation (e.g., Blackman, Cann, Janssen, & Smith, 1998; Cann, Blackman, Smith, & McAllister, 1997). There is an adjacent basaltic block (to the east) interpreted to be the hanging wall of the detachment fault, and seafloor is covered by a thin drape of variably lithified sediment, volcanic deposits, and rubble. Atlantis Massif also hosts the Lost City Hydrothermal Field (LCHF), which discharges alkaline fluids rich in hydrogen and methane derived from serpentinization reactions (Kelley et al., 2005).

4.2.2.2.4.2 Petrology and Alteration

Hole U1309D was drilled 14–15 km west of the MAR axis and 5 km north of the LCHF, penetrating the Atlantis massif to 1415.5 mbsf, and recovering 75% of the cored interval (Expedition 304/305 Scientists, 2006b). The basement is divided into 770 units comprising dominantly crustal rock types, including dike-/sill-related basalt and dolerite (~3%) and gabbroic rocks (~91%). Interlayered with these are several olivine-rich rock types (~5%; dunites, wehrlites, troctolites). A few thin mantle peridotite intervals are also present in the upper 180 msb (Blackman et al., 2011; Expedition 304/305 Scientists, 2006b).

The gabbbroic rocks are mainly gabbros, including gabbronorite and orthopyroxene-bearing gabbro, making up 55.7% of the core. Olivine-bearing to troctolitic gabbro (25.5%) is the second most abundant rock type, followed by troctolite and other olivine-rich rocks (8%) and oxide gabbro (7%). Contact relations suggest that gabbro is generally intrusive into the more olivine-rich rocks (olivine gabbro and troctolite), and that the gabbroic rocks are intruded by felsic dikes and oxide gabbro. Subhorizontal sheets or sills of diabase intruded other rocks at several depths late in the intrusive history of the site. The abundance of dikes in the uppermost 100 m of Hole U1309D may imply that the detachment fault rooted in the dike–gabbro transition zone (McCaig & Harris, 2012). The gabbroic rocks are primitive, having Mg numbers of 67–87, and may be cumulates related through crystal fractionation to the diabases, which are tholeiitic basalt and minor basaltic andesite.

The fault zone of the detachment is represented by fragments of brecciated talc-tremolite fault schist and fractured metadiabase as deep as 100 mbsf in Holes U1309B and U1309D (Expedition 304/305 Scientists, 2006b). Paleomagnetic data indicate flexural clockwise rotation of the footwall <1 Ma along a ridge parallel horizontal axis (Morris et al., 2009). Logging data, low core recovery, and cataclasis at 108–126 mbsf and 685–785 mbsf indicate fault zones. The core is divided into three structural units based on these and another zone of cataclasis and crystal-plastic deformation.

Site U1310 lies in the hanging wall ~10 km west of the rift valley axis and ~600 m east of the termination of the detachment fault exposed on the central dome (Expedition 304/305 Scientists, 2006c). Hole U1310B recovered olivine + plagioclase phyric, pillow basalt fragments from the uppermost 13.5 m of basement having N-MORB compositions. Site U1311 is located near the termination of the detachment fault and may lie either in the hanging wall or in a klippe atop the footwall (Expedition 304/305 Scientists, 2006d). Drilling in Hole U1311A penetrated into fresh, moderately plagioclase-olivine phyric pillow basalt (with 13% recovery), which is similar in composition to rocks recovered from Site U1310.

Seawater–rock interactions manifest in core from Hole U1309D range from granulite to zeolite facies and alteration assemblages and vein fillings record the unroofing and uplift of the Atlantis Massif (Blackman et al., 2011; Nozaka, Fryer, & Andreani, 2008). Alteration intensity is highly variable, but generally decreases downhole. Commonly, sections of core reveal retrograde overprinting of earlier high-temperature metamorphism by later low-grade conditions. Alteration intensity is a function of time-integrated fluid flow, but also depends on the nature of the rocks. For instance, olivine gabbros and troctolites are more reactive than gabbro, because of the strong contrast in chemical potentials between olivine and plagioclase (e.g., Frost, Beard, McCaig, & Condliffe, 2008). Given the lithological heterogeneity of the basement at Site 1309, it is difficult to link the extent of alteration to the intensity of flow of seawater-derived fluids.

The history of alteration began with the dynamic recrystallization of olivine, clinopyroxene, plagioclase, and brown hornblende under granulite to upper amphibolite-facies conditions during mylonitic deformation (Blackman et al., 2011). Breakdown of clinopyroxene to hornblende under amphibolite-facies conditions is localized in and around sparse mylonitic deformation zones. The continued inflow of seawater-derived fluids led to increasing background alteration facilitated by the generation of microcracks, which helped to distribute fluids across a large volume of rock. This static background alteration is most pronounced in the uppermost 300 m of the basement and decreases in intensity downhole. Actinolitic hornblende and secondary plagioclase (±epidote) formed in the gabbros and oxide gabbros, whereas olivine-rich lithologies grew chlorite-tremolite(±talc) coronas along olivine-plagioclase grain boundaries. When the system had cooled to lower greenschist-facies temperatures, olivine underwent serpentinization, driving alteration of plagioclase to prehnite and hydrogrossular

in olivine-rich lithologies (Frost et al., 2008). Chlorite-tremolite ± talc rocks are developed in the uppermost 25 m of basement, where strain localization took place along the detachment. Late-stage prehnite to zeolite-facies veins have saponite + zeolite, zeolite, carbonate, and occasional anhydrite. These veins do not show a systematic relation to high-temperature deformation or lithology. They are likely related to the recent and rapid uplift of Atlantis Massif (e.g.,Nozaka & Fryer, 2011; Nozaka et al., 2008). Thermochrolonological data (Schoolmeesters et al., 2012) indicate that the entire section in Hole U1309D cooled to 780 °C around the same time (0.8 Ma), and then the uppermost 600 m of basement cooled faster than the deeper section, probably because of seawater convection in the damage zone of the footwall.

4.2.2.2.4.3 Geophysical Measurements

The upper 94 m of basement penetration was logged in Hole U1309B, and measurements extended to >1400 msb in Hole U1309D (Expedition 304/305 Scientists, 2006b). Hole U1309D was revisited for additional logging during Expedition 340T (Expedition 340T Scientists, 2012). Wireline tools deployed in these holes included natural gamma ray emission, bulk density, electrical resistivity, neutron porosity, sonic velocity, borehole temperature, and formation imaging. In addition, detailed vertical seismic profile experiments were completed to assist with correlation between regional and borehole geophysical data.

Hole conditions were generally very good to excellent throughout the cored interval, and core recovery was high, allowing direct interpretation of differences in log response in terms of primary or secondary lithology and structure (Expedition 304/305 Scientists, 2006b). Natural gamma ray emissions are generally low in the rocks of Site U1309, but there are thin zones of elevated values. One of these natural gamma anomalies (near 750 mbsf) corresponds to an abrupt increase in formation electrical resistivity, and an increase (and reduction of variability) in bulk density. That change in geophysical properties is associated with an interval containing up to 20% of basalt diabase, in contrast to overlying and underlying intervals comprising mainly gabbro and gabbronorite. Formation resistivity decreases again at 1100 mbsf. Sonic velocities generally increase with depth into the crust, although there are local excursions where lower velocities generally correlate with lower bulk density and electrical resistivity.

Borehole imaging data (electrical and sonic) suggest that small intervals of borehole enlargement often correspond to open faults and fractures. Comparison of core and geophysical logging data shows a strong correlation between deviations in logging parameters (e.g., lower bulk density and sonic velocity) and the intensity and pervasiveness of alteration. There are also good correlations between physical properties determined in the borehole, on recovered core, and inferred from seismic reflection studies.

Logging data collected in Hole U1309D during Expedition 340T are generally consistent with data collected during earlier expeditions, except for the temperature log (Blackman, Slagle, Guerin, & Harding, 2014). Much of the deepest

half of the hole had warmed toward a predrilling state, but there was gentle downward curvature in the gradient from the upper 750 mbsf, and small local excursions in downhole temperature near 750 and 1100 mbsf, corresponding to abrupt changes in geophysical properties. Larger excursions in temperature at these depths were also apparent in Expedition 305 data (Expedition 304/305 Scientists, 2006b), but these were superimposed on an overall profile indicative of borehole cooling. These zones could have been more intensively invaded by cool drilling fluids when the holes were cored, and thus would have taken longer to recover. There may be slow fluid convection within the upper 750 msb in this crustal section today, helping to steepen the geothermal gradient in the upper half of Hole 1309D (Blackman et al., 2014). There is no rapid flow down Hole 1309D today, as this would suppress the borehole thermal gradient much more than observed (e.g., Winslow et al., 2013), but slow flow of water down the hole and into thin zones at depth (fractures, faults), could also explain the observed curvature.

4.2.2.3 SYNTHESIS: METHOD AND SITE COMPARISONS AND TRENDS

4.2.2.3.1 Hydrogeologic Properties of the Ocean Crust

A compilation of direct hydrogeologic measurements made during DSDP, ODP, and IODP (Figure 4.2.2.6) illustrates both consistent trends and notable data gaps. Data and interpretations from packer measurements and analyses of thermal logs were added to the global data set during IODP from 3.5-my-old crust on the eastern flank of the Juan de Fuca Ridge, in Holes U1301A, U1301B, and U1362A (Becker & Fisher, 2000; 2008; Becker et al., 2013; Winslow et al., 2013). Collectively these data suggest that the highest permeability within basaltic upper crust is found within the upper 300 msb, particularly within lithologically defined zones that are tens of meters thick (as opposed to the uppermost crust as a whole). Data from 0.9 to 3.6 my-old seafloor in this area suggest that the highest permeabilities are found in upper crust of the youngest sites (Becker & Davis, 2003), but there is considerable variability associated with the scale (test duration), type, and depth range of measurements. Permeability data are sparse below the upper 300 m of the crust, and there is a notable lack of data from a crust older than 8 my (Figure 4.2.2.6). Direct measurements of permeability in gabbroic rocks characteristic of the middle to lower crust have been made during scientific drilling only in Hole 735B (Becker, 1991), and only one set of measurements has been made in fast-spread basaltic crust, in Hole 801C, the oldest site in the data set (Larson, Fisher, Jarrard, & Becker, 1993) (Figure 4.2.2.6).

Permeability calculated from the cross-hole response observed in Hole 1027C to long-term flow down Hole U1301B (Figure 4.2.2.4(A)) is at the lower end of estimates based on single-hole packer experiments (Becker & Fisher, 2000; Becker et al., 2013; Fisher et al., 2008) (Figure 4.2.2.6). This is surprising

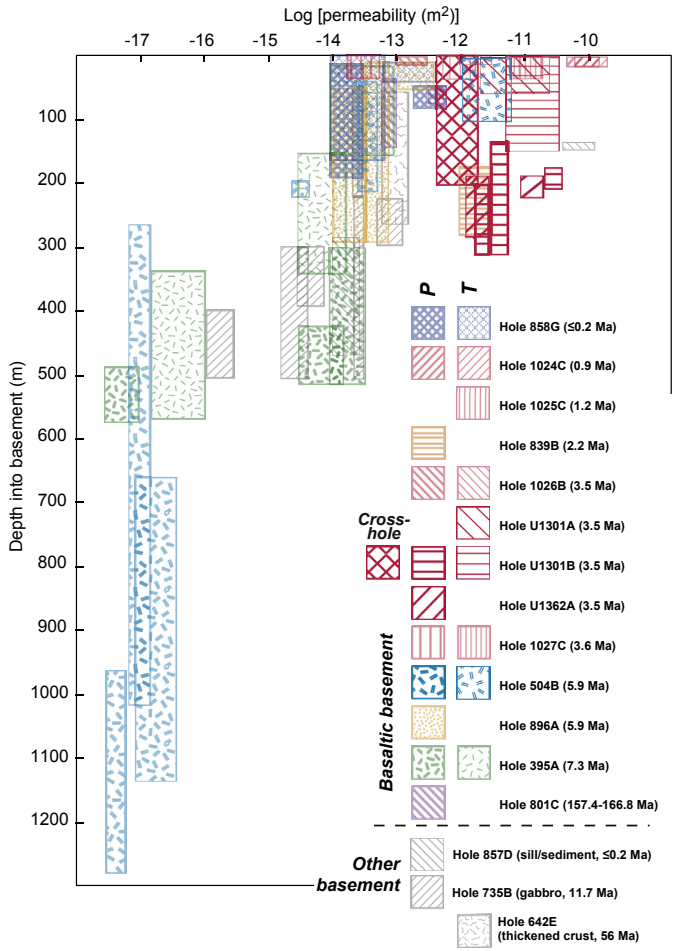

FIGURE 4.2.2.6 Compilation of borehole measurements of permeability in the volcanic ocean crust *(based on summary presented in Becker and Fisher (2008), with additional data from Fisher et al. (2008), Becker et al. (2013), and Winslow et al. (2013))*. Most data are from packer experiments (P) and borehole thermal logs (T), but there was a single cross-hole test, as discussed in the text. Black and white version: Data collected during DSDP and ODP are shown in gray with patterns. Color version: Data collected during DSDP, ODP, and IODP are coded by color and pattern, with DSDP and ODP data being partly transparent.

at first because the long-term cross-hole response should be influenced by a much larger rock volume, extending perhaps 10–30 km from the borehole, and larger test volumes generally correspond to higher apparent permeability in heterogeneous/fractured rock systems such as the ocean crust (e.g., Clauser, 1992; Fisher, 1998; Guéguen, Gavrilenko, & Le Ravalec, 1996). Basement permeability estimated from this cross-hole response is also one to three orders of

magnitude lower than estimates based on numerical modeling and calculations based on tidal responses and drainage following tectonic strain events, which evaluated similar crustal volumes (Davis & Becker, 2002; 2004; Davis et al., 2004, 1997; Wang, He, & Davis, 1997).

One possible explanation for the differences in inferred properties based on these methods is that permeability in the crust around Sites U1301 and 1027 is azimuthally anisotropic. Anisotropy in the seismic properties of oceanic basement rocks is thought to result from preferential orientation of cracks, faults, and fractures (i.e., the crustal "fabric") (e.g., Sohn, Webb, Hildebrand, & Cornuelle, 1997; Stephen, 1981). The dominant crustal fabric is generally thought to be subparallel to the orientation of the mid-ocean ridge where the crust was created. This fabric may favor fluid flow in the crust in the "along-strike" direction (Delaney, Robigou, McDuff, & Tivey, 1992; Haymon et al., 1991; Wilcock & Fisher, 2004), an interpretation consistent with geochemical and thermal data from the Expedition 301/327 field area (Fisher, Davis, et al., 2003; Hutnak et al., 2006; Walker, McCarthy, Fisher, & Guilderson, 2007; Wheat, Elderfield, Mottl, & Monnin, 2000). Azimuthal anisotropy could influence the permeability apparent from a cross-hole experiment involving a single observation borehole (Figure 4.2.2.4(B)). If the angle of measurement is oblique relative to the direction of greatest permeability (as between Holes U1301B and 1027C), the measured value will be very close to that in the lowest-permeability direction, even for a large anisotropy ratio. Confirmation that the crust in this area is azimuthally anisotropic with respect to permeability requires simultaneous monitoring of pressure changes in response to pumping or free flow using two or more observation boreholes at significantly different azimuths from the perturbation borehole.

Along-strike consistency of crustal hydrologic properties in this area, at a kilometer scale, is indicated from comparison of packer and wireline logging responses, and rates of drilling penetration, from Holes U1301B and U1362A (Becker et al., 2013; Expedition 301 Scientists, 2005a; Expedition 327 Scientists, 2011a). Similar consistency is not apparent in crustal layering on the basis of core descriptions, but this may result from local heterogeneity at the hand-sample scale and/or limited recovery from the upper crust. New analyses of borehole thermal logs suggest surprising consistency in bulk permeability of the uppermost crust (Winslow et al., 2013), but the global data set remains sparse.

4.2.2.3.2 The Integrated Record of Fluid–Rock Interactions in the Ocean Crust

The distribution and style of low-temperature alteration seen in volcanic sections of oceanic crust cored by IODP are generally similar to those sampled by ODP and DSDP, including the presence of secondary minerals and their distribution in veins, alteration halos, and "background" alteration (e.g., Alt, 2004; Bach, Humphris, & Fisher, 2004). IODP drilling provides valuable new insights

regarding lithological controls on alteration in upper oceanic basement and the relation between alteration and crustal spreading rate.

Prior to drilling Hole 1256D it was believed that oxidation effects (as evidenced by reddish alteration halos) should generally decrease with depth in the volcanic section of oceanic crust (e.g., Figure 4.2.2.3, Hole 504B). Hole 1256D does not show this trend with depth. Instead, alteration halos are focused in distinct zones, indicating a strong control on fluid flow by lithology and permeability, and halos are much less abundant in this hole than in crust formed at intermediate spreading rates (Figure 4.2.2.3). In some cases, oxidation and alteration effects are concentrated at the tops of lava flows or eruptive units, which can be rubbly and permeable, allowing focused fluid flow. IODP drilling and logging of cores by shipboard scientists has extended this comparison to crust generated at slow-spreading ridges, showing that alteration halos there are comparable in abundance to those in crust formed at intermediate spreading rates (Figure 4.2.2.3).

Analysis of samples and data from ODP/IODP Site 1256 has also shown that sheet flows are more abundant throughout the volcanic section in crust formed at fast spreading rates, whereas pillows are more abundant at intermediate and slow rates (Figure 4.2.2.3) (Expedition 309/312 Scientists, 2006b; Teagle & Wilson, 2007). This interpretation is consistent with observations made of seafloor lava flows (e.g., Carbotte & Scheirer, 2004), and may help to explain the extreme efficiency of crustal cooling where the crust was formed at a fast-spreading ridge (Fisher, Stein, et al., 2003; Hutnak et al., 2008). At the other extreme, basaltic upper crust may be thinner or absent on slow- and ultraslow-spreading seafloor (e.g., Dick, Lin, & Schouten, 2003; Ildefonse et al., 2007).

A thorough understanding of the distribution of rock types found in oceanic crustal sections is limited by biased and incomplete recovery of core, but careful integration with geophysical logs can put core samples in context, as demonstrated by Tominaga et al. (2009) (Figure 4.2.2.7). Their analysis of wireline logs from Hole 1256D, with an emphasis on resistivity and natural gamma ray responses, suggests that breccias and fragmented flows comprise more than 50% of the borehole interval. In contrast, the vast majority (>90%) of recovered core was classified as sheet and massive basalt flows.

A comparison of age trends in physical properties from multiple DSDP, ODP, and IODP holes using core and wireline logging data illustrates how measurements made at different scales may be related, and how the crust ages (Bartetzko & Fisher, 2008) (Figure 4.2.2.8). Sonic velocity, electrical resistivity, bulk density, and total gamma ray measured with wireline tools in open boreholes in the upper basaltic crust tend to increase with basement age, whereas sonic velocity and bulk density measured on core samples tend to decrease. Properties determined from wireline data and core data tend to converge with increasing crustal age. One explanation for these observations is that borehole-scale measurements record the infilling of small pore spaces by alteration products of water–rock interaction. In contrast, hand samples tend to become less dense

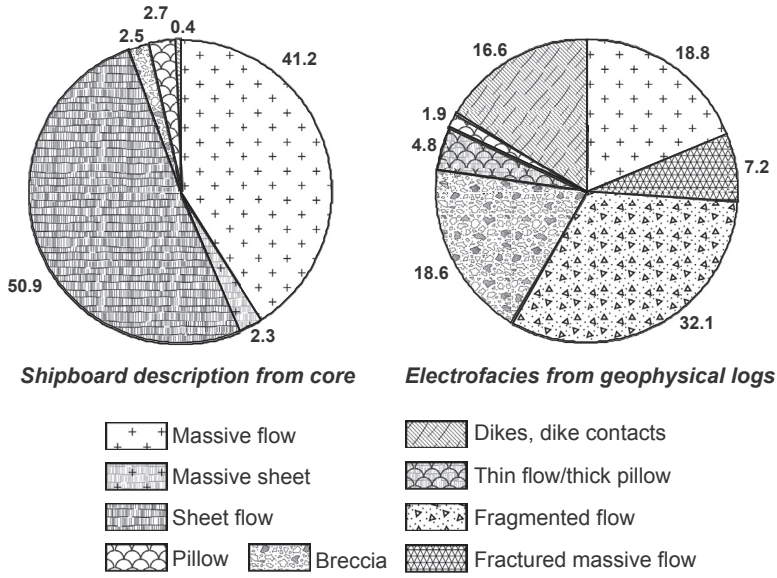

FIGURE 4.2.2.7 Comparison of rock types in the volcanic section of Hole 1256D indicated by shipboard core descriptions (left) and analysis of electrofacies (geophysical logs) to identify igneous stratigraphy (right) *(modified from Tominaga et al. (2009))*. Pie slices and numbers indicate the percent of each rock type identified. Shipboard lithostratigraphic data were tabulated from visual core descriptions from Leg 206, Expedition 309 and 312 (Expedition 309/312 Scientists, 2006b; Shipboard Scientific Party, 2003) by calculating a total of recovered core length of each rock type divided by a total of recovered core length. Recovery was highly variable, but was particularly low in zones containing breccia and heavily fractured rock.

and have lower sonic velocities as a result of the same alteration processes, as expressed in the mostly massive samples that are recovered during coring.

Results of hydrogeologic experiments in basement can be inconsistent with alteration patterns in recovered crustal rocks. For example, in Holes U1301B and U1362A, the highest transmissivity occurs at 150–180 mbsf (Figure 4.2.2.6), but alteration halos are abundant throughout the basement sections (Figure 4.2.2.3). Upper basement temperature in this area is ~65 °C, but carbonates in veins from these holes formed at temperatures of 30–40 °C (Coggon, Teagle, Cooper, & Vanko, 2004; Coggon et al., 2010). The difference between present and past temperatures likely results from a relatively recent reduction in the rate of fluid circulation in this setting, as local basement outcrops were systematically buried during the Pleistocene, and basement temperatures warmed in response to reduced heat extraction (Hutnak & Fisher, 2007).

The oceanic crust is a significant global sink for carbon, and carbonate is more abundant in the volcanic section of crust formed at slow spreading rates than in upper crust formed at intermediate and fast spreading rates (Alt & Teagle, 1999; Gillis & Coogan, 2011). Vein carbonates recovered from core samples of

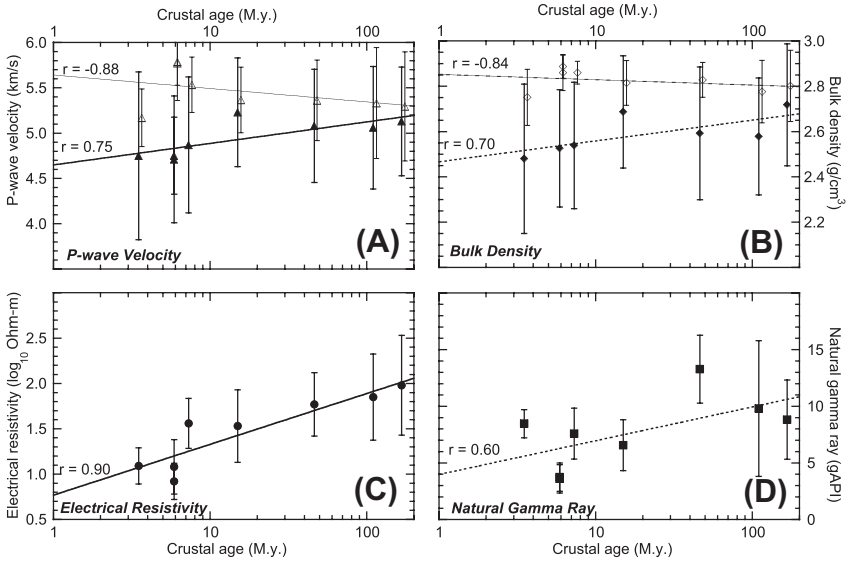

FIGURE 4.2.2.8 Comparison of geophysical logging (borehole) and physical properties (hand sample) values from the upper ocean crustal sections as a function of basement age *(updated from Bartetzko & Fisher (2008))*, based on selected data from DSDP, ODP, and IODP boreholes. Data are from Holes U1301, 504B, 896A, 395A, 1256D, 1224F, 418A, and 801C, with means of borehole logging data plotted using filled symbols and means of core data plotted using open symbols. Lines are least squares best fits based on a semilogarithmic trend (but note $\log_{10}$ scale for electrical resistivity values) with correlation coefficients shown. Solid lines are significant with >99% confidence (Bartetzko & Fisher, 2008).

the oceanic crust are valuable recorders of fluid chemical evolution as the seafloor ages, indicating variations in both crustal and seawater composition and temperature (e.g., Expedition 301 carbonates, Coggon et al., 2004, 2010; Gillis & Coogan, 2011; Rausch, Böhm, Bach, Klügel, & Eisenhauer, 2013).

The temperature of water–rock interaction also has an important influence on the composition of crustal fluids, as shown with a global compilation of data from modern upper basement fluids (Fisher & Wheat, 2010) (Figure 4.2.2.9), including analyses of sedimentary pore fluids recovered from adjacent to the sediment–basement contact (e.g., Elderfield, Wheat, Mottl, Monnin, & Spiro et al., 1999; Mottl, 1989; Orcutt et al., 2013). For major ions involved in mainly inorganic exchange (e.g., magnesium), there is relatively little change in fluid composition at temperatures below about 20 °C, but solutes involved in biogeochemical cycling (e.g., phosphate) show evidence of reaction at essentially all fluid temperatures (Figure 4.2.2.9). In some cases, reactions may occur in both basement rocks and in overlying sediments, with diffusional exchange between crustal and sedimentary layers.

Alteration in core samples from Hole 1256D indicates an abrupt increase in the thermal gradient with depth (Figure 4.2.2.5), corresponding to an increase in alteration temperature across the transition from lavas to dikes, similar to

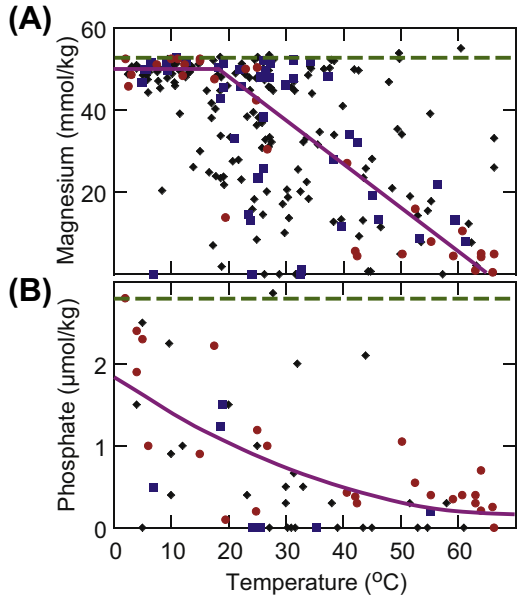

FIGURE 4.2.2.9 Concentrations of magnesium and phosphate in ridge-flank fluids from the upper portion of basaltic basement plotted versus measured and inferred temperatures at the sediment–basement contact *(figure modified from Fisher & Wheat (2010))*. These plots are based on a global compilation of DSDP, ODP, and IODP data, and analyses of samples collected with traditional gravity and piston corers, and from seafloor seeps and springs. Data are classified to indicate quality. Black and white version: circle = highest quality; square = moderate quality; diamond = fair quality. Horizontal dashed lines indicate typical concentrations in bottom seawater. Solid lines/curves show global trends based on the highest quality data. Color version: red circle = highest quality; blue square = moderate quality; black diamond = fair quality. Green dashed lines indicate typical concentrations in bottom seawater. Pink solid lines/curves show global trends based on the highest quality data.

that documented in DSDP/ODP Hole 504B and at Pito Deep (Alt et al., 2010; Alt et al., 1996; Heft, Gillis, Pollock, Karson, & Klein, 2008). This observation indicates different styles of fluid circulation at depth, controlled by lithology and permeability, with higher-temperature hydrothermal fluids in the dikes and cooler seawater fluids in the volcanic section at the spreading axis, and continued low-temperature circulation in the lavas on the ridge flank. Cores from Hole 1256D also reveal a step in the thermal gradient at the dike-plutonic boundary, corresponding to contact metamorphism of the lowermost dikes driven by intrusion of underlying gabbros near the spreading axis (Alt et al., 2010; Koepke et al., 2008).

Studies of lower crustal rocks from Hole 735B, the deepest seafloor penetration into plutonic rocks, showed that metamorphism, fracturing, and fluid penetration occurred over a wide range of conditions (Bach et al., 2001; Dick et al., 2000). Results from gabbroic rocks from Hole 1309D generally show a similar

range of alteration styles, from granulite and amphibolite-facies reactions down to low-temperature smectite formation (Blackman et al., 2011). However, the extent of granulite facies alteration is greater and Sr isotope compositions are less altered in the uppermost 400 m of Hole 735B (McCaig, Delacour, Fallick, Castelain, & Früh-Green, 2010), suggesting less cumulative seawater–rock interaction in comparison to Hole 1309D. In addition, cores from Hole U1309D have a greater abundance of olivine-rich rocks, making serpentinization reactions especially important, and they lack evidence for subgreenschist conditions. Nozaka et al. (2008) interpret this to indicate rapid uplift of the Atlantis Massif (Hole U1309D) in comparison to Atlantis Bank (Hole 735B), but there could also be different fracturing histories during cooling. This would be consistent with packer testing results from Hole 735B, which suggested considerable permeability at present (Becker, 1991), but temperature logs from Hole U1309D suggest limited fluid circulation (Blackman et al., 2014).

4.2.2.3.3 Future Needs and Frontiers

The observations and interpretations presented in this chapter remain limited by the numbers and locations of boreholes that penetrate into the igneous oceanic crust (Figure 4.2.2.2). There are consistent trends in hydrogeologic properties and crustal structure and alteration at many sites (for example, heterogeneity in properties associated with crustal layering). Although scientific ocean drilling is filling gaps across the global map, resolving dependencies on seafloor age and spreading rate will require additional opportunities to sample, analyze, and test crustal conditions and quantify histories of water–rock interaction. Researchers also need access to multiple basement holes separated by a range of distances, to assess the consistency and continuity of properties. This is often not done during scientific ocean drilling because of the cost and time required to establish, drill, sample, test, and instrument basement holes; results from individual holes raise questions about whether these sample points are representative, and how properties and processes may vary laterally, with age, and with proximity to features such as fracture zones and seamounts. These questions can be addressed, in part, by drilling age transects to assess the evolution of ocean crust as a result of fluid–rock interactions.

There are ongoing experiments, results of which are currently incomplete, that were designed to test the nature of permeability and advective transport in upper basement on the eastern flank of the Juan de Fuca Ridge. In 2011, after the new CORKs installed during Expedition 327 were permitted to equilibrate for a year following drilling, a large-diameter ball valve was opened on the wellhead of the CORK in Hole U1362B. Downhole temperature loggers and a flowmeter attached to the discharging wellhead were deployed to assess the rate at which fluids discharged from the overpressured formation for the next 2 years, and the long-term pressure response from surrounding CORKs will help to determine both crustal-scale properties and the extent of permeability anisotropy (vertical, azimuthal). In addition, about 500 m^3 of fluid and tracers

(gas, solute, particles) were injected into the formation around Hole U1362B in 24 h as part of a cross-hole tracer experiment initiated during IODP Expedition 327. Multiyear records of tracer recovery are being developed from fluids collected with Osmosamplers and active pumping systems deployed on multiple CORK wellheads before and after tracer injection. Additional records from Osmosamplers and temperature loggers were recovered in Summer 2014.

Drilling deeper basement holes remains important for exploration of hydrothermal processes and effects in the crust. Further drilling in Hole 1256D (or elsewhere) through the uppermost gabbros will allow testing of petrological and geophysical models for melt lenses at mid-ocean ridges. Such drilling will also enable testing of how hydrothermal metamorphism, fluid fluxes, and heat transport in high-temperature axial hydrothermal systems are related throughout the crust, and help reconcile budgets for hydrothermal heat, fluid fluxes, and chemical fluxes. Drilling in nearby ("pilot") holes can be helpful for assessing lithologic and alteration heterogeneity, and could facilitate cross-hole tests that measure rock properties and fluid flow at the scale of crustal fluid flow and in multiple directions. Reconciling present-day hydrologic conditions and the integrated history of water–rock interaction through the crust requires the collection of physical and chemical core samples and borehole data from the same locations, across a range of spatial scales, through long crustal sections. Colocated multidisciplinary studies have long been a strength of scientific ocean drilling, and will continue to be essential in the future, as new tools, methods, and opportunities are developed.

ACKNOWLEDGMENTS

This research used data provided by the Ocean Drilling Program (ODP) and the Integrated Ocean Drilling Program (IODP) and was supported by National Science Foundation grants OCE 1031808, OCE-1131210, OCE-1260408 (AF), and OCE-1129631 and OCE-1334758 (JA), and Consortium for Ocean Leadership Projects T327A7 and T327B7 (ATF). This manuscript benefitted from thoughtful reviews by D. Blackman, A. McCaig, and R. Harris. This is C-DEBI contribution 228.

REFERENCES

Alt, J. C. (2004). Alteration of the upper oceanic crust: mineralogy, chemistry, and processes. In E. E. Davis, & H. Elderfield (Eds.), *Hydrogeology of the oceanic lithosphere* (pp. 456–488). Cambridge, UK: Cambridge University Press.

Alt, J. C., Laverne, C., Coggon, R. M., Teagle, D. A. H., Banerjee, N. R., Morgan, S., et al. (2010). Subsurface structure of a submarine hydrothermal system in ocean crust formed at the East Pacific Rise. *Geochemistry, Geophysics, Geosystems*, *11*(10), Q10010. http://dx.doi.org/10.1029/2010GC003144.

Alt, J. C., & Shanks, W. C., III (2011). Microbial sulfate reduction and the sulfur budget for a complete section of altered oceanic basalts, IODP Hole 1256D (eastern Pacific). *Earth Planet. Sci. Lett*, *310*, 73–83. http://dx.doi.org/10.1016/j.epsl.2011.1007.1027.

Alt, J. C., & Teagle, A. H. (1999). The uptake of carbon during alteration of ocean crust. *Geochimica Cosmochimica et Acta*, *63*, 1527–1535.

Alt, J. C., & Teagle, D. A. H. (2003). Hydrothermal alteration of upper oceanic crust formed at a fast spreading ridge: mineral, chemical, and isotopic evidence from ODP Site 801. *Chemical Geology*, *201*(3–4), 191–211.

Alt, J. C., Teagle, D. A. H., Laverne, C., Vanko, D. A., Bach, W., Honnorez, J., et al. (1996). Ridge-flank alteration of upper oceanic crust in the Eastern Pacific: synthesis of results for volcanic rocks of Holes 504B and 896A. In J. C. Alt, H. Kinoshita, & L. Stokking (Eds.), *Proceedings of the ocean drilling program, science results 148* (pp. 435–452). College Station, TX: Ocean Drilling Program.

Bach, W., Alt, J. C., Niu, Y., Humphris, S. E., Erzinger, J., & Dick, H. J. B. (2001). The geochemical consequences of late-stage low-grade alteration of lower ocean crust at the SW Indian Ridge: results from ODP Hole 735B (Leg 176). *Geochimica Cosmochimica et Acta*, *65*, 3,267–263,287.

Bach, W., Humphris, S. E., & Fisher, A. T. (2004). Fluid flow and fluid-rock interaction within oceanic crust: reconciling geochemical, geological and geophysical observations. In W. S. D. Wilcock, E. Delong, D. Kelley, J. A. Baross, & S. C. Cary (Eds.), *Subseafloor biosphere at mid-ocean ridges* (pp. 99–117). Washington, D. C: AGU Geophysical Monograph 144, American Geophysical Union. http://dx.doi.org/10.1029/144GM07.

Bartetzko, A., & Fisher, A. T. (2008). Physical properties of young (3.5 m.y.) oceanic crust from the eastern flank of Juan de Fuca Ridge: comparison of wireline and core measurements with global data. *Journal of Geophysical Research*, B05105. http://dx.doi.org/10.1029/2007JB005268.

Bartetzko, A., Pezard, P., Goldberg, D., Sun, Y.-F., & Becker, K. (2001). Volcanic stratigraphy of DSDP/ODP Hole 395A: an interpretation using well-logging data. *Marine Geophysical Researches*, *22*, 111–127.

Becker, K. (1986). Special report: development and use of packers in ODP. *JOIDES Journal*, *12*, 51–57.

Becker, K. (1991). In-situ bulk permeability of oceanic gabbros in Hole 735B, ODP Leg 118. In R. P. Von Herzen, & P. T. Robinson (Eds.), *Proceedings of the ocean drilling program, science results 118* (pp. 333–347). College Station, TX: Ocean Drilling Program.

Becker, K., Bartetzko, A., & Davis, E. E. (2001). Leg 174B synopsis: revisiting Hole 395A for logging and long-term monitoring of off-axis hydrothermal processes in young oceanic crust. In K. Becker, & M. J. Malone (Eds.), *Proceedings of the ocean drilling program, science results 174B* (pp. 1–12). College Station, TX: Ocean Drilling Program.

Becker, K., & Davis, E. (2003). New evidence for age variation and scale effects of permeabilities of young oceanic crust from borehole thermal and pressure measuements. *Earth and Planetary Science Letters*, *201*(3–4), 499–508.

Becker, K., & Davis, E. (2004). In situ determinations of the permeability of the igneous oceanic crust. In E. E. Davis, & H. Elderfield (Eds.), *Hydrogeology of the oceanic lithosphere* (pp. 189–224). Cambridge, UK: Cambridge University Press.

Becker, K., & Davis, E. E. (2005). A review of CORK designs and operations during the Ocean Drilling Program. In A. T. Fisher, T. Urabe, A. Klaus, & the Expedition 327 Scientists (Eds.), *Proc. IODP 301*. Tokyo: Integrated Ocean Drilling Program Management International, Inc. http://dx.doi.org/10.2204/iodp.proc.301.104.

Becker, K., & Fisher, A. T. (2000). Permeability of upper oceanic basement on the eastern flank of the Endeavor Ridge determined with drill-string packer experiments. *Journal of Geophysical Research*, *105*(B1), 897–912.

Becker, K., & Fisher, A. T. (2008). Borehole tests at multiple depths resolve distinct hydrologic intervals in 3.5-Ma upper oceanic crust on the eastern flank of the Juan de Fuca Ridge. *Journal of Geophysical Research*, *113*, B07105. http://dx.doi.org/10.1029/2007JB005446.

Becker, K., Fisher, A. T., & Tsuji, T. (2013). New packer experiments and borehole logs in upper oceanic crust: evidence for ridge-parallel consistency in crustal hydrogeologic properties. *Geochemistry, Geophysics, Geosystems*, *14*. (8). http://dx.doi.org/10.1002/ggge.20201.

Becker, K., Langseth, M., Von Herzen, R. P., & Anderson, R. (1983). Deep crustal geothermal measurements, hole 504B, Costa Rica rift. *Journal of Geophysical Research*, *88*, 3447–3457.

Becker, K., Langseth, M. G., & Hyndman, R. D. (1984). Temperature measurements in hole 395A, leg 78B. In R. Hyndman, & M. Salisbury (Eds.), *Init. Repts., DSDP* (pp. 689–698). Washington, D. C: 78B, U. S. Govt. Printing Office.

Blackman, D. K., Cann, J. R., Janssen, B., & Smith, D. K. (1998). Origin of extensional core complexes: evidence from the Mid-Atlantic Ridge at Atlantis Fracture Zone. *Journal of Geophysical Research*, *103*(B9), 21,315–321,333.

Blackman, D. K., Ildefonse, B., John, B. E., Ohara, Y., Miller, D. J., Abe, N, et al. (2011). Drilling constraints on lithospheric accretion and evolution at Atlantis Massif, Mid-Atlantic Ridge 30°N. *Journal of Geophysical Research: Solid Earth*, *116*(B7), B07103. http://dx.doi.org/10.1029/2010jb007931.

Blackman, D. K., Slagle, A., Guerin, G., & Harding, A. (2014). Geophysical signatures of pasrt and present hydration within a young oceanic core complex. *Geophysical Research Letters*, *41*, 1179–1186.

Cann, J. R., Blackman, D. K., Smith, D. K., & McAllister, E. (1997). Corrugated slip surfaces formed at ridge-transform intersections on the mid-atlantic ridge. *Nature*, *385*, 329–331.

Carbotte, S., & Scheirer, D. S. (2004). Variability of ocean crustal structure created along the global mid-ocean ridge. In E. E. Davis, & H. Elderfield (Eds.), *Hydrogeology of the oceanic lithosphere* (pp. 59–107). Cambridge, UK: Cambridge University Press.

Clauser, C. (1992). Permeability of crystalline rocks, Transactions. *American Geophysical Union*, *73*(233), 237–238.

Coggon, R. M., Teagle, D. A. H., Cooper, M. J., & Vanko, D. A. (2004). Linking basement carbonate vein composition to porewater geochemistry across the eastern flank of the Juan de Fuca Ridge, ODP Leg 168. *Earth and Planetary Science Letters*, *219*, 111–128.

Coggon, R. M., Teagle, D. A. H., Smith-Duque, C. E., Alt, J. C., & Cooper, M. J. (2010). Reconstructing past seawater Mg/Ca and Sr/Ca from mid-ocean ridge flank calcium carbonate veins. *Science*, *327*(5969), 1114–1117.

Davis, E. E., & Becker, K. (2002). Observations of natural-state fluid pressures and temperatures in young oceanic crust and inferrences regarding hydrothermal circulation. *Earth and Planetary Science Letters*, *204*, 231–248.

Davis, E. E., & Becker, K. (2004). Observations of temperature and pressure: constraints on ocean crustal hydrologic state, properties, and flow. In E. E. Davis, & H. Elderfield (Eds.), *Hydrogeology of the oceanic lithosphere* (pp. 225–271). Cambridge, UK: Cambridge University Press.

Davis, E. E., Becker, K., Dziak, R. P., Cassidy, J. F., Wang, K., & Lilley, M. (2004). Hydrologic response to a seafloor spreading episode on the Juan de Fuca Ridge: evidence for co-seismic net crustal dilation. *Nature*, *430*, 335–338.

Davis, E. E., Becker, K., Pettigrew, T., Carson, B., & MacDonald, R. (1992). CORK: a hydrologic seal and downhole observatory for deep-ocean boreholes. In E. E. Davis, M. Mottl, & A. T. Fisher (Eds.), *Proceedings of the ocean drilling program, initial reports 139* (pp. 43–53). College Station, TX: Ocean Drilling Program.

Davis, E. E., Chapman, D. S., Mottl, M. J., Bentkowski, W. J., Dadey, K., Forster, C., et al. (1992). FlankFlux: an experiment to study the nature of hydrothermal circulation in young oceanic crust. *Canadian Journal of Earth Sciences*, *29*(5), 925–952.

Davis, E. E., Chapman, D. S., Wang, K., Villinger, H., Fisher, A. T., Robinson, S. W., et al. (1999). Regional heat-flow variations across the sedimented Juan de Fuca Ridge eastern flank: constraints on lithospheric cooling and lateral hydrothermal heat transport. *Journal of Geophysical Research*, *104*(B8), 17,675–617,688.

Davis, E. E., LaBonte, A., He, J., Becker, K., & Fisher, A. T. (2010). Thermally stimulated "runaway" downhole flow in a super-hydrostatic ocean-crustal borehole: observations, simulations, and inferences regarding crustal permeability. *Journal of Geophysical Research*, *115*, B07102. http://dx.doi.org/10.1029/2009JB006986.

Davis, E. E., Wang, K., He, J., Chapman, D. S., Villinger, H., & Rosenberger, A. (1997). An unequivocal case for high Nusselt-number hydrothermal convection in sediment-buried igneous oceanic crust. *Earth and Planetary Science Letters*, *146*, 137–150.

Delaney, J. R., Robigou, V., McDuff, R., & Tivey, M. (1992). Geology of a vigorous hydrothermal system on the Endeavor segment, Juan de Fuca Ridge. *Journal of Geophysical Research*, *97*, 19,663–619,682.

Dick, H. J. B., Lin, J., & Schouten, H. (2003). An ultraslow-spreading class of ocean ridge. *Nature*, *426*(6965), 405–412.

Dick, H. J. B., Natland, J. H., Alt, J. C., Bach, W., Bideau, D., Gee, J. S., et al. (2000). A long in situ section of the lower ocean crust; results of ODP Leg 176 drilling at the Southwest Indian Ridge. *Earth and Planetary Science Letters*, *179*, 31–51.

Edwards, K. J., Wheat, C. G., Orcutt, B. N., Hulme, S., Becker, K., Jannasch, H., et al. (2012). Design and deployment of borehole observatories and experiments during IODP Expedition 336, Mid-Atlantic Ridge flank at North Pond. In K. J. Edwards, W. Bach, A. Klaus, & the Expedition 336 Scientists (Eds.), *Proceedings of the integrated ocean drilling program 336*. Tokyo: Integrated Ocean Drilling Program Management International, Inc. http://dx.doi.org/10.2204/iodp.proc.336.109.2012.

Elderfield, H., Wheat, C. G., Mottl, M. J., Monnin, C., & Spiro, B. (1999). Fluid and geochemical transport through oceanic crust: a transect across the eastern flank of the Juan de Fuca Ridge. *Earth and Planetary Science Letters*, *172*, 151–165.

Escartín, J., Smith, D. K., Cann, J., Schouten, H., Langmuir, C. H., & Escrig, S. (1998). Central role of detachment faults in accretion of slow-spreading oceanic lithosphere. *Nature*, *455*, 790–795.

Expedition 301 Scientists. (2005a). Expedition 301 summary. In A. T. Fisher, T. Urabe, A. Klaus, & the Expedition 301 Scientists (Eds.), *Proceedings of the integrated ocean drilling program 301*. Tokyo: Integrated Ocean Drilling Program Management International, Inc. http://dx.doi.org/10.2204/iodp.proc.301.101.2005.

Expedition 301 Scientists. (2005b). Site U1301. In A. T. Fisher, T. Urabe, A. Klaus, & the Expedition 301 Scientists (Eds.), *Proceedings of the integrated ocean drilling program 301*. Tokyo: IIntegrated Ocean Drilling Program Management International, Inc. http://dx.doi.org/10.2204/iodp.proc.301.106.2005.

Expedition 304/305 Scientists. (2006a). Expedition 304/305 summary. In D. K. Blackman, B. Ildefonse, B. E. John, Y. Ohara, D. J. Miller, C. J. MacLeod, et al. (Eds.), *Proceedings of the integrated ocean drilling program 304/305*. Tokyo: Integrated Ocean Drilling Program Management International, Inc. http://dx.doi.org/10.2204/iodp.proc.304305.101.2006.

Expedition 304/305 Scientists. (2006b). Site U1309. In D. K. Blackman, B. Ildefonse, B. E. John, Y. Ohara, D. J. Miller, C. J. MacLeod, et al. (Eds.), *Proceedings of the integrated ocean drilling program 304/305*. Tokyo: Integrated Ocean Drilling Program Management International, Inc. http://dx.doi.org/10.2204/iodp.proc.304305.103.2006.

Expedition 304/305 Scientists. (2006c). Site U1310. In D. K. Blackman, B. Ildefonse, B. E. John, Y. Ohara, D. J. Miller, C. J. MacLeod, et al. (Eds.), *Proceedings of the integrated ocean drilling program 304/305*. Tokyo: Integrated Ocean Drilling Program Management International, Inc. http://dx.doi.org/10.2204/iodp.proc.304305.104.2006.

Expedition 304/305 Scientists. (2006d). Site U1311. In D. K. Blackman, B. Ildefonse, B. E. John, Y. Ohara, D. J. Miller, C. J. MacLeod, et al. (Eds.), *Proceedings of the integrated ocean drilling program 304/305*. Tokyo: Integrated Ocean Drilling Program Management International, Inc. http://dx.doi.org/10.2204/iodp.proc.304305.105.2006.

Expedition 309/312 Scientists. (2006a). Expedition 309/312 summary. In D. A. H. Teagle, J. C. Alt, S. Umino, S. Miyashita, N. R. Banerjee, D. S. Wilson, et al. (Eds.), *Proceedings of the integrated ocean drilling program 309/312*. Tokyo: Integrated Ocean Drilling Program Management International, Inc. http://dx.doi.org/10.2204/iodp.proc.309312.101.2006.

Expedition 309/312 Scientists. (2006b). Site 1256. In D. A. H. Teagle, J. C. Alt, S. Umino, S. Miyashita, N. R. Banerjee, D. S. Wilson, et al. (Eds.), *Proceedings of the integrated ocean drilling program 309/312*. Tokyo: Integrated Ocean Drilling Program Management International, Inc. http://dx.doi.org/10.2204/iodp.proc.309312.103.2006.

Expedition 327 Scientists. (2011a). Expedition 327 summary. In A. T. Fisher, T. Tsuji, K. Petronotis, & the Expedition 327 Scientists (Eds.), *Proceedings of the integrated ocean drilling program 327*. Tokyo: Integrated Ocean Drilling Program Management International, Inc. http://dx.doi.org/10.2204/iodp.proc.327.101.2011.

Expedition 327 Scientists. (2011b). Site U1301. In A. T. Fisher, T. Tsuji, K. Petronotis, & the Expedition 327 Scientists (Eds.), *Proceedings of the integrated ocean drilling program 327*. Tokyo: Integrated Ocean Drilling Program Management International, Inc. http://dx.doi.org/10.2204/iodp.proc.327.104.2011.

Expedition 327 Scientists. (2011c). Site U1362. In A. T. Fisher, T. Tsuji, K. Petronotis, & the Expedition 327 Scientists (Eds.), *Proceedings of the integrated ocean drilling program 327*. Tokyo: Integrated Ocean Drilling Program Management International, Inc. http://dx.doi.org/10.2204/iodp.proc.327.103.2011.

Expedition 327 Scientists. (2011d). Site U1363. In A. T. Fisher, T. Tsuji, K. Petronotis, & the Expedition 327 Scientists (Eds.), *Proceedings of the integrated ocean drilling program 327*. Tokyo: Integrated Ocean Drilling Program Management International, Inc. http://dx.doi.org/10.2204/iodp.proc.327.106.2011.

Expedition 335 Scientists. (2012). Site 1256. In D. A. H. Teagle, B. Ildefonse, P. Blum, & the Expedition 335 Scientists (Eds.), *Proceedings of the integrated ocean drilling program 335*. Tokyo: Integrated Ocean Drilling Program Management International, Inc. http://dx.doi.org/10.2204/iodp.proc.335.103.2012.

Expedition 336 Scientists. (2012a). Expedition 336 summary. In K. J. Edwards, W. Bach, A. Klaus, & the Expedition 336 Scientists (Eds.), *Proceedings of the integrated ocean drilling program 336*. Tokyo: Integrated Ocean Drilling Program Management International, Inc. http://dx.doi.org/10.2204/iodp.proc.336.101.2012.

Expedition 336 Scientists. (2012b). Site 395. In K. J. Edwards, W. Bach, A. Klaus, & the Expedition 336 Scientists (Eds.), *Proceedings of the integrated ocean drilling program 336*. Tokyo: Integrated Ocean Drilling Program Management International, Inc. http://dx.doi.org/10.2204/iodp.proc.336.103.2012.

Expedition 336 Scientists. (2012c). Site U1382. In K. J. Edwards, W. Bach, A. Klaus, & the Expedition 336 Scientists (Eds.), *Proceedings of the integrated ocean drilling program 336*. Tokyo: Integrated Ocean Drilling Program Management International, Inc. http://dx.doi.org/10.2204/iodp.proc.336.104.2012.

Expedition 336 Scientists. (2012d). Site U1383. In K. J. Edwards, W. Bach, A. Klaus, & the Expedition 336 Scientists (Eds.), *Proceedings of the integrated ocean drilling program 336*. Tokyo: Integrated Ocean Drilling Program Management International, Inc. http://dx.doi.org/10.2204/iodp.proc.336.105.2012.

Expedition 340T Scientists. (2012). *Atlantis massif oceanic core complex: Velocity, porosity, and impedance contrasts within the domal core of atlantis massif: Faults and hydration of lithosphere during core complex evolution, IODP Preliminary Report 340T*. College Station, TX: Integrated Ocean Drilling Program Management International, Inc. http://dx.doi.org/10.2204/iodp.pr.340T.2012.

Fisher, A. T. (1998). Permeability within basaltic oceanic crust. *Reviews of Geophysics*, *36*(2), 143–182.

Fisher, A. T. (2010). IODP Expedition 321T: cementing operations at Hole U1301A and U1301B, eastern flank of the Juan de Fuca Ridge Sci. *Drilling*, *9*. http://dx.doi.org/10.2204/iodp.sd.9.02.2010.

Fisher, A. T., Becker, K., & Davis, E. E. (1997). The permeability of young oceanic crust east of Juan de Fuca Ridge determined using borehole thermal measurements. *Geophysical Research Letters*, *24*, 1311–1314.

Fisher, A. T., Davis, E. E., & Becker, K. (2008). Borehole-to-borehole hydrologic response across 2.4 km in the upper oceanic crust: implications for crustal-scale properties. *Journal of Geophysical Research*, *113*, B07106. http://dx.doi.org/10.1029/2007JB005447.

Fisher, A. T., Davis, E. E., Hutnak, M., Spiess, V., Zühlsdorff, L., Cherkaoui, A., et al. (2003). Hydrothermal recharge and discharge across 50 km guided by seamounts on a young ridge flank. *Nature*, *421*, 618–621.

Fisher, A. T., Stein, C. A., Harris, R. N., Wang, K., Silver, E. A., Pfender, M., et al. (2003). Abrupt thermal transition reveals hydrothermal boundary and role of seamounts within the Cocos Plate. *Geophysical Research Letters*, *30*(11), 1550. http://dx.doi.org/10.1029/2002GL016766.

Fisher, A. T., Tsuji, T., Petronotis, K., & the Expedition 327 Scientists (2011). *Proceedings of the integrated ocean drilling program expedition reports 327*. Tokyo: Integrated Ocean Drilling Program Management International, Inc. http://dx.doi.org/10.2204/iodp.proc.327.2011.

Fisher, A. T., Tsuki, T., Petronotis, K., Wheat, C. G., Becker, K., Clark, J. F., & IODP Expedition 327 Scientific Party, & Atlantis Expedition AT18-07 Scientific Party., et al. (2012). Installing and servicing borehole crustal observatories to run three-dimensional cross-hole perturbation and monitoring experiments on the eastern flank of the Juan de Fuca Ridge: IODP Expedition 327 and Atlantis Expedition AT18-07. *Scientific Drilling*, *13*. http://dx.doi.org/10.2204/iodp.sd.13.01.2011.

Fisher, A. T., Urabe, T., Klaus, A., & the Expedition 301 Scientists (2005). *Proceedings of the integrated ocean drilling program 301*. Tokyo: Integrated Ocean Drilling Program Management International, Inc. http://dx.doi.org/10.2204/iodp.proc.301.2005.

Fisher, A. T., & Wheat, C. G. (2010). Seamounts as conduits for massive fluid, heat, and solute fluxes on ridge flanks. *Oceangraphy*, *23*(1), 74–87.

Fisher, A. T., Wheat, C. G., Becker, K., Cowen, J., Orcutt, B., Hulme, S., et al. (2011). Design, deployment, and status of borehole observatory systems used for single-hole and cross-hole experiments, IODP Expedition 327, eastern flank of the Juan de Fuca Ridge. In A. T. Fisher, T. Tsuji, K. Petronotis, & the Expedition 327 Scientists (Eds.), *Proceedings of the integrated ocean drilling program 327*. Tokyo: Integrated Ocean Drilling Program-Management International, Inc. http://dx.doi.org/10.2204/iodp.proc.327.107.2011.

Fisher, A. T., Wheat, C. G., Becker, K., Davis, E. E., Jannasch, H., Schroeder, D., et al. (2005). Scientific and technical design and deployment of long-term, subseafloor observatories for hydro-

geologic and related experiments, IODP Expedition 301, eastern flank of Juan de Fuca Ridge. In A. T. Fisher, T. Urabe, A. Klaus, & the Expedition 301 Scientists (Eds.), *Proceedings of the integrated ocean drilling program 301*. Tokyo: Integrated Ocean Drilling Program Management International, Inc. http://dx.doi.org/10.2204/iodp.proc.301.103.2005.

France, L., Ildefonse, B., & Koepke, J. (2009). Interactions between magma and hydrothermal system in Oman ophiolite and in IODP Hole 1256D: Fossilization of a dynamic melt lens at fast spreading ridges. *Geochemistry, Geophysics, Geosystems*, *10*, Q10O19. http://dx.doi.org/10.1029/2009GC002652.

Frost, B. R., Beard, J. S., McCaig, A. M., & Condliffe, E. (2008). The formation of micro-rodingites from IODP Hole U1309D: key to understanding th process of serpentinization. *JP*, *49*(9), 1579–1588.

Gable, R., Morin, R. H., & Becker, K. (1992). Geothermal state of DSDP Holes 333A, 395A and 534A: results from the dianaut program. *Geophysical Research Letters*, *19*, 505–508.

Gao, Y., Vils, F., Cooper, K. M., Banerjee, N., Harris, M., Hoefs, J., et al. (2012). Downhole variation of lithium and oxygen isotopic compositions of oceanic crust at East Pacific Rise, ODP Site 1256. *Geochemistry, Geophysics, Geosystems*, *13*(10), Q10001. http://dx.doi.org/10.1029/2012GC004207.

Gillis, K., & Coogan, L. A. (2011). Secular variation in carbon uptake into the ocean crust. *Earth and Planetary Science Letters*, *302*, 385–392.

Guéguen, Y., Gavrilenko, P., & Le Ravalec, M. (1996). Scales of rock permeability. *Surveys in Geophysics*, *17*, 245–263.

Haymon, R. M., Fornari, D. J., Edwards, M. H., Carbotte, S., Wright, D., & Macdonald, K. C. (1991). Hydrothermal vent distribution along the East Pacific Rise crest (9° 09'-54' N) and its relationship to magmatic and tectonic processes on fast-spreading mid-ocean ridges. *Earth and Planetary Science Letters*, *104*, 513–534.

Heft, K. L., Gillis, K. M., Pollock, M. A., Karson, J. A., & Klein, E. M. (2008). Role of upwelling hydrothermal fluids in the development of alteration patterns at fast spreading ridges: evidence from the sheeted dike complex at Pito Deep. *Geochemistry, Geophysics, Geosystems*, *9*, Q05O07. http://dx.doi.org/10.1029/2007GC001926.

Huber, J. A., Butterfield, D. A., Johnson, H. P., & Baross, J. A. (2006). Microbial life in ridge flank crustal fluids. *Environmental Microbiology*, *88*, 88–99.

Hutnak, M., & Fisher, A. T. (2007). The influence of sedimentation, local and regional hydrothermal circulation, and thermal rebound on measurements of heat flux from young seafloor. *Journal of Geophysical Research*, *112*, B12101. http://dx.doi.org/10.1029/2007JB005022.

Hutnak, M., Fisher, A. T., Harris, R., Stein, C., Wang, K., Spinelli, G., et al. (2008). Large heat and fluid fluxes driven through mid-plate outcrops on ocean crust. *Nature Geoscience, 1*. http://dx.doi.org/10.1038/ngeo264.

Hutnak, M., Fisher, A. T., Zühlsdorff, L., Spiess, V., Stauffer, P., & Gable, C. W. (2006). Hydrothermal recharge and discharge guided by basement outcrops on 0.7-3.6 Ma seafloor east of the Juan de Fuca Ridge: observations and numerical models. *Geochemistry, Geophysics, Geosystems*, *7*. http://dx.doi.org/10.1029/2006GC001242.

Ildefonse, B., Blackman, D. K., John, B. E., Ohara, Y., Miller, D. J., & MacLeod, C. J. (2007). Oceanic core complexes and crustal accretion at slow-spreading ridges. *Geology*, *35*(7), 623–626.

Johnson, H. P., & Pruis, M. J. (2003). Fluxes of fluid and heat from the oceanic crustal reservoir. *Earth and Planetary Science Letters*, *216*, 565–574.

Kelley, D. S., Karson, J. A., Fruh-Green, G. L., Yoerger, D. R., Shank, T. M., Butterfield, D. A., et al. (2005). A serpentinite-hosted ecosystem: the lost city hydrothermal field. *Science*, *307*(5714), 1428–1434.

Koepke, J., Christie, D. M., Dziony, W., Holtz, F., Lattard, D., Maclennan, J., et al. (2008). Petrography of the dike-gabbro transition at IODP Site 1256 (equatorial Pacific): the evolution of the granoblastic dikes. *Geochemistry, Geophysics, Geosystems*, *9*, Q07O09. http://dx.doi.org/10.1029/2008GC001939.

Koepke, J., France, L., Müller, T., Faure, F., Goetze, N., Dziony, W., et al. (2011). Gabbros from IODP Site 1256, equatorial Pacific: Insight into axial magma chamber processes at fast spreading ocean ridges. *Geochemistry, Geophysics, Geosystems*, *12*(9), Q09014. http://dx.doi.org/10.1029/2011GC003655.

Langseth, M. G., Becker, K., Von Herzen, R. P., & Schultheiss, P. (1992). Heat and fluid flux through sediment on the western flank of the Mid-Atlantic Ridge: a hydrogeological study of North Pond. *Geophysical Research Letters*, *19*, 517–520.

Langseth, M. G., & Herman, B. (1981). Heat transfer in the oceanic crust of the Brazil Basin. *Journal of Geophysical Research*, *86*, 10805–10819.

Langseth, M. G., Hyndman, R. D., Becker, K., Hickman, S. H., & Salisbury, M. H. (1984). The hydrogeological regime of isolated sediment ponds in mid-oceanic ridges. In R. H. Hyndman, & M. H. Salisbury (Eds.), *Init. Repts., DSDP* (pp. 825–837). Washington, D.C.: 78B, U. S. Govt. Printing Office.

Larson, R. L., Fisher, A. T., Jarrard, R., & Becker, K. (1993). Highly permeable and layered Jurassic oceanic crust in the western Pacific. *Earth and Planetary Science Letters*, *119*, 71–83.

Lawrence, J. R., & Gieskes, J. M. (1981). Constraints on water transport and alteration in the oceanic crust from the isotopic composition of pore water. *Journal of Geophysical Research*, *86*, 7924–7934.

Lesem, L. B., Greytok, F., Marotta, F., & McKetta, J. J., Jr. (1957). A method of calculating the distribution of temperature in flowing gas wells. *Petroleum Transactions of AIME*, *210*, 169–176.

Lever, M. A., Rouxel, O., Alt, J. C., Shimizu, N., Ono, S., Coogon, R. M., et al. (2013). Evidence for microbial carbon and sulfur cycling in deeply buried ridge flank basalt. *Science*, *339*. (6125). http://dx.doi.org/10.1126/science.1229240.

Lucazeau, F., Bonneville, A., Escartin, J., Von Herzen, R. P., Gouze, P., Carton, H., et al. (2006). Heat flow variations on a slowly accreting ridge: constraints on the hydrothermal and conductive cooling for the Lucky Strike segment (Mid-Atlantic Ridge, 37 N). *Geochemistry, Geophysics, Geosystems*, *7*. http://dx.doi.org/10.1029/2005GC001178.

Matthews, M., Salisbury, M., & Hyndman, R. (1984). Basement logging on the Mid-Atlantic Ridge, deep sea drilling project hole 395A. In R. D. Hyndman, & M. H. Salisbury (Eds.), *Init. Repts., DSDP* (pp. 717–730). Washington, D.C.: 78B, U. S. Govt. Printing Office.

McCaig, A. M., Delacour, A. G., Fallick, A. E., Castelain, T., & Früh-Green, G. L. (2010). Detachment fault control on hydrothermal circulation systems: Interpreting the subsurface beneath the TAG hydrothermal field using the isotopic and geological evolution of oceanic core complexes in the Atlantic. In P. A. Rona, C. W. Devey, J. Dyment, & B. Murton (Eds.), *Diversity of hydrothermal systems on slow spreading ocean ridges* (pp. 207–240). Washington DC: AGU Geophysical Monograph 108, American Geophysical Union.

McCaig, A. M., & Harris, A. C. (2012). Hydrothermal circulation and the dike-gabbro transition in the detachment mode of slow seafloor spreading. *Geology*, *40*, 367–370.

Moos, D. (1990). Petrophysical results from logging in DSDP Hole 395A, ODP Leg 109. In R. Detrick, & J. Honnorez (Eds.), *Proceedings of the ocean drilling program, scientific results 106/109* (pp. 237–253). College Station, TX: Ocean Drilling Program.

Morin, R. H., Hess, A. E., & Becker, K. (1992). In situ measurements of fluid flow in DSDP Holes 395A and 534A: results from the Dianaut program. *Geophysical Research Letters*, *19*, 509–512.

Morin, R. H., Moos, D., & Hess, A. E. (1992). Analysis of the borehole televiewer log from DSDP 395A: results from the Dianaut program. *Geophysical Research Letters*, *19*, 501–504.

Morris, A., Gee, J. S., Pressling, N., John, B. E., MacLeod, C. J., Grimes, C. B., et al. (2009). Footwall rotation in an oceanic core complex quantified using reoriented Integrated Ocean Drilling Program core samples. *Earth and Planetary Science Letters*, *287*, 217–228.

Mottl, M. J. (1989). Hydrothermal convection, reaction and diffusion in sediments on the Costa Rica Rift flank, pore water evidence from ODP Sites 677 and 678. In K. Becker, & H. Sakai (Eds.), *Proceedings of the ocean drilling program, scientific results 111* (pp. 195–214). College Station, TX: Ocean Drilling Program.

Mottl, M. J. (2003). Partitioning of energy and mass fluxes between mid-ocean ridge axes and flanks at high and low temperature. In P. Halbach, V. Tunnicliffe, & J. Hein (Eds.), *Energy and mass transfer in submarine hydrothermal systems* (pp. 271–286). Berlin, Germany: DWR 89, Dahlem University Press.

Nozaka, T., & Fryer, P. (2011). Alteration of the oceanic lower crust at a slow-spreading axis: Insight from vein-related zoned halos in olivine gabbro from Atlantis Massif, Mid-Atlantic Ridge. *Journal of Petroleum*, *52*, 643–664. http://dx.doi.org/10.1093/petrology/egq098.

Nozaka, T., Fryer, P., & Andreani, M. (2008). Formation of clay minerals and exhumation of lower-crustal rocks at Atlantis Massif, Mid-Atlantic Ridge. *Geochemistry, Geophysics, Geosystems*, *9*(11), Q11005. http://dx.doi.org/10.1029/2008GC002207.

Ono, S., Keller, N., Rouxel, O., & Alt, J. C. (2012). Sulfur-33 constraints on the origin of secondary pyrite in altered ocean basement rocks. *Geochimica Cosmochimica et Acta*, *87*, 323–340.

Orcutt, B. N., Wheat, C. G., Rouxel, O., Hulme, S., Edwards, K. J., & Bach, W. (2013). Oxygen consumption rates in subseafloor basaltic crust derived from a reaction transport model. *Nature Communications*, *4*. http://dx.doi.org/10.1038/ncomms3539.

Parsons, B., & Sclater, J. G. (1977). An analysis of the variation of ocean floor bathymetry and heat flow with age. *Journal of Geophysical Research*, *82*, 803–829.

Rausch, S., Böhm, F., Bach, W., Klügel, A., & Eisenhauer, A. (2013). Calcium carbonate veins in ocean crust record increases in seawater Mg/Ca and Sr/Ca within the past 30 million years. *Earth and Planetary Science Letters*, *362*, 215–224. http://dx.doi.org/10.1016/j.epsl.2012.12.005.

Rouxel, O., Shanks, W. C. I., Bach, W., & Edwards, K. J. (2008). Integrated Fe and S isotope study of seafloor hydrothermal vents at East Pacific Rise 9-10°N. *Chem Geol*, *252*, 214–227.

Ryan, W. B. F., Carbotte, S. M., Coplan, J. O., O'Hara, S., Melkonian, A., Arko, R., et al. (2009). Global multi-resolution topography synthesis. *Geochemistry, Geophysics, Geosystems*, *10*(3), Q03014. http://dx.doi.org/10.1029/2008GC002332.

Schoolmeesters, N., Cheadle, M. J., John, B. E., Reiners, P. W., Gee, J., & Grimes, C. B. (2012). The cooling history and the depth of the detachment faulting at the Atlantis Massif oceanic core complex. *Geochemistry, Geophysics, Geosystems*, *13*, 1–19.

Shipboard Scientific Party. (1979). Site 395. In W. G. Melson, & P. D. Rabinowitz (Eds.), *Deep sea drilling project, initial reports 45* (pp. 131–264). Washington, D.C: U. S. Govt. Printing Office.

Shipboard Scientific Party. (1997a). Introduction and summary: hydrothermal circulation in the oceanic crust and its concequences on the eastern flank of the Juan de Fuca Ridge. In E. E. Davis, A. T. Fisher, & J. Firth (Eds.), *Proceedings of the ocean drilling program, initial reports 168* (pp. 7–21). College Station, TX: Ocean Drilling Program.

Shipboard Scientific Party. (1997b). Rough basement transect (Sites 1026 and 1027). In E. E. Davis, A. T. Fisher, & J. Firth (Eds.), *Proceedings of the ocean drilling program, initial reports 168* (pp. 101–160). College Station, TX: Ocean Drilling Program.

Shipboard Scientific Party. (2003). Site 1256. In D. S. Wilson, D. A. H. Teagle, & G. D. Acton (Eds.), *Proceedings of the ocean drilling program, initial reports 206*. College Station, TX, USA: Ocean Drilling Program. http://dx.doi.org/10.2973/odp.proc.ir.206.103.2003.

Sohn, R. A., Webb, S. C., Hildebrand, J. A., & Cornuelle, B. C. (1997). Three-dimensional tomographic velocity structure of upper crust, CoAxial segment, Juan de Fuca Ridge: implications for on-axis evolution and hydrothermal circulation. *Journal of Geophysical Research*, *102*, 17,679–617,695.

Spinelli, G. A., & Fisher, A. T. (2004). Hydrothermal circulation within rough basement on the Juan de Fuca Ridge flank. *Geochemistry, Geophysics, Geosystems*, *5*(2), Q02001. http://dx.doi.org/10.1029/2003GC000616.

Stein, C. A., Stein, S., & Pelayo, A. M. (1995). Heat flow and hydrothermal circulation. In S. E. Humphris, R. A. Zierenberg, L. S. Mullineaux, & R. E. Thompson (Eds.), *Seafloor hydrothermal Systems: Physical, chemical, biological and geological interactions Geophysical monograph series: Vol. 91*. (pp. 425–445). Washington, D.C.: American Geophysical Union.

Stein, J. S., & Fisher, A. T. (2003). Observations and models of lateral hydrothermal circulation on a young ridge flank: numerical evaluation of thermal and chemical constraints. *Geochemistry, Geophysics, Geosystems*, *4*. http://dx.doi.org/10.1029/2002GC000415.

Stephen, R. (1981). Seismic anisotropy observed upper oceanic crust. *Geophysical Research Letters*, *8*, 865–868.

Swift, S. A., Reichow, M., Tikku, A., Tominaga, M., & Gilbert, L. (2008). Velocity structure of upper ocean crust at Ocean Drilling Program Site 1256. *Geochemistry, Geophysics, Geosystems*, *9*(10), Q10O13. http://dx.doi.org/10.1029/2008GC002188.

Teagle, D. A. H., & Wilson, D. S. (2007). Leg 206 Synthesis: Initiation of drilling an intact section of upper oceanic crust formed at a superfast spreading rate at Site 1256 in the eastern equatorial Pacific. In D. S. Wilson, D. A. H. Teagle, G. D. Acton, & D. A. Vanko (Eds.), *Proceedings of the ocean drilling program, initial reports 206* (pp. 1–7). College Station, TX, USA: Ocean Drilling Program. http://dx.doi.org/10.2973/odp.proc.sr.206.001.2007.

Tominaga, M., Teagle, D. A. H., Alt, J. C., & Umino, S. (2009). Determination of the volcanostratigraphy of oceanic crust formed at superfast spreading ridge: electrofacies analyses of ODP/IODP Hole 1256D. *Geochemistry, Geophysics, Geosystems*, *10*. (9). http://dx.doi.org/10.1029/2008GC002143.

Villinger, H., Grevemeyer, I., Kaul, N., Hauschild, J., & Pfender, M. (2002). Hydrothermal heat flux through aged oceanic crust: where does the heat escape? *Earth and Planetary Science Letters*, *202*(1), 159–170.

Walker, B. D., McCarthy, M. D., Fisher, A. T., & Guilderson, T. P. (2007). Dissolved inorganic carbon isotopic composition of low-temperature axial and ridge-flank hydrothermal fluids of the Juan de Fuca Ridge. *Marine Chemistry*, *108*. http://dx.doi.org/10.1016/j.marchem.2007.11.002.

Wang, K., He, J., & Davis, E. E. (1997). Influence of basement topography on hydrothermal circulation in sediment-buried oceanic crust. *Earth and Planetary Science Letters*, *146*, 151–164.

Wheat, C. G., Edwards, K. J., Pettigrew, T., Jannasch, H. W., Becker, K., Davis, E. E., et al. (2012). CORK-Lite: Bringing legacy boreholes back to life. *Scientific Drilling*, *14*. http://dx.doi.org/10.2204/iodp.sd.2214.2205.2012.

Wheat, C. G., Elderfield, H., Mottl, M. J., & Monnin, C. (2000). Chemical composition of basement fluids within an oceanic ridge flank: implications for along-strike and across-strike hydrothermal circulation. *Journal of Geophysical Research*, *105*(B6), 13437–13447.

Wheat, C. G., Jannasch, H., Fisher, A. T., Becker, K., Sharkey, J., & Hulme, S. M. (2010). Subseafloor seawater-basalt-microbe reactions: continuous sampling of borehole fluids in a ridge flank environment. *Geochemistry, Geophysics, Geosystems*, Q07011. http://dx.doi.org/10.1029/2010GC00305.

Wheat, C. G., Jannasch, H., Kastner, M., Hulme, S., Cowen, J., Edwards, K., et al. (2011). Fluid sampling from oceanic borehole observatories: design and methods for CORK activities (1990-2010). In A. T. Fisher, T. Tsuji, K. Petronotis, & the Expedition 327 Scientists (Eds.), *Proceedings of the integrated ocean drilling program 327*. Tokyo: Integrated Ocean Drilling Program Management International, Inc. http://dx.doi.org/10.2204/iodp.proc.327.109.2011.

Wheat, C. G., McManus, J., Mottl, M., & Giambalvo, E. G. (2003). Oceanic phosphorus imbalance: magnitude of the mid-ocean ridge flank hydrothermal sink. *Geophysical Research Letters, 30*. http://dx.doi.org/10.1029/2003GL017318.

Wheat, C. G., Mottl, M. J., Fisher, A. T., Kadko, D., Davis, E. E., & Baker, E. (2004). Heat and fluid flow through a basaltic outcrop on a ridge flank. *Geochemistry, Geophysics, Geosystems*, *5*. (12). http://dx.doi.org/10.1029/2004GC000700.

Wilcock, W. S. D., & Fisher, A. T. (2004). Geophysical constraints on the sub-seafloor environment near mid-ocean ridges. In W. S. D. Wilcock, E. Delong, D. Kelley, J. A. Baross, & S. C. Cary (Eds.), *Subseafloor biosphere at mid-ocean ridges* (pp. 51–74). Washington, D.C: AGU Geophysical Monograph 144, American Geophysical Union. http://dx.doi.org/10.1029/144GM05.

Winslow, D. M., Fisher, A. T., & Becker, K. (2013). Characterizing borehole fluid flow and formation permeability in the ocean crust using linked analytic models and Markov Chain Monte Carlo analysis. *Geochemistry, Geophysics, Geosystems*, *14*. (9). http://dx.doi.org/10.1002/ggge.20241.

Ziebis, W., McManus, J., Ferdelman, T., Schmidt-Schierhorn, F., Bach, W., Muratli, J., et al. (2012). Interstitial fluid chemistry of sediments underlying the North Atlantic gyre and the influence of subsurface fluid flow. *Earth and Planetary Science Letters*, *323-324*, 79–91.

Zühlsdorff, L., Hutnak, M., Fisher, A. T., Spiess, V., Davis, E. E., Nedimovic, M., et al. (2005). Site Surveys related to IODP Expedition 301: ImageFlux (SO149) and RetroFlux (TN116) expeditions and earlier studies. In A. T. Fisher, T. Urabe, & A. Klaus (Eds.), *Proceedings of the integrated ocean drilling program 301*. Tokyo: Integrated Ocean Drilling Program Management International, Inc. http://dx.doi.org/10.2204/iodp.proc.301.102.2005.

DEVELOPMENTS IN MARINE GEOLOGY 7

EARTH AND LIFE PROCESSES DISCOVERED FROM SUBSEAFLOOR ENVIRONMENTS

A DECADE OF SCIENCE ACHIEVED BY THE INTEGRATED OCEAN DRILLING PROGRAM (IODP)

R. STEIN, D. BLACKMAN, F. INAGAKI AND H.-C. LARSEN

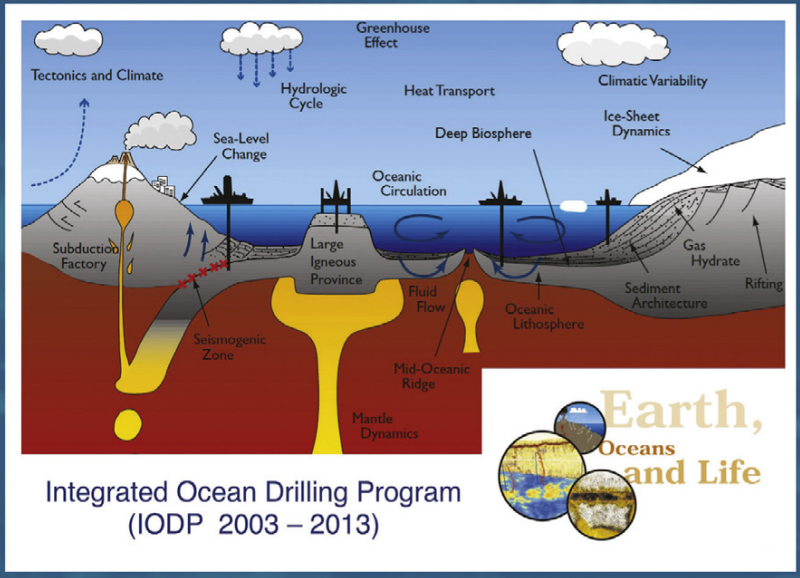

SERIES EDITOR: R. STEIN

Developments in Marine Geology

Volume 7

Earth and Life Processes Discovered from Subseafloor Environments

Developments in Marine Geology

Volume 7

Earth and Life Processes Discovered from Subseafloor Environments

A Decade of Science Achieved by the Integrated Ocean Drilling Program (IODP)

Edited by

Ruediger Stein
Division of Geosciences, Alfred Wegener Institute for Polar and Marine Research, Bremerhaven, Germany

Donna K. Blackman
Scripps Institution of Oceanography, University of California San Diego, La Jolla, CA, USA

Fumio Inagaki
Kochi Institute for Core Sample Research, Japan Agency for Marine-Earth Science & Technology (JAMSTEC), Nankoku, Kochi, Japan

Hans-Christian Larsen

ELSEVIER

AMSTERDAM • BOSTON • HEIDELBERG • LONDON
NEW YORK • OXFORD • PARIS • SAN DIEGO
SAN FRANCISCO • SINGAPORE • SYDNEY • TOKYO

Elsevier
Radarweg 29, PO Box 211, 1000 AE Amsterdam, Netherlands
The Boulevard, Langford Lane, Kidlington, Oxford OX5 1GB, UK
225 Wyman Street, Waltham, MA 02451, USA

First edition 2014

Notices

Knowledge and best practice in this field are constantly changing. As new research and experience broaden our understanding, changes in research methods, professional practices, or medical treatment may become necessary.

Practitioners and researchers must always rely on their own experience and knowledge in evaluating and using any information, methods, compounds, or experiments described herein. In using such information or methods they should be mindful of their own safety and the safety of others, including parties for whom they have a professional responsibility.

To the fullest extent of the law, neither the Publisher nor the authors, contributors, or editors, assume any liability for any injury and/or damage to persons or property as a matter of products liability, negligence or otherwise, or from any use or operation of any methods, products, instructions, or ideas contained in the material herein.

ISBN: 978-0-444-62617-2
ISSN: 1572-5480